

Multi-energy microgrid optimal operation

Chen, Yumin

2019

Chen, Y. (2019). Multi-energy microgrid optimal operation. Master's thesis, Nanyang Technological University, Singapore.

<https://hdl.handle.net/10356/136774>

<https://doi.org/10.32657/10356/136774>

This work is licensed under a Creative Commons Attribution-NonCommercial 4.0 International License (CC BY-NC 4.0).

Downloaded on 09 Apr 2024 11:08:29 SGT



**NANYANG
TECHNOLOGICAL
UNIVERSITY**

SINGAPORE

MULTI-ENERGY MICROGRID OPTIMAL OPERATION

CHEN YUMIN

SCHOOL OF ELECTRICAL & ELECTRONIC ENGINEERING

2019

MULTI-ENERGY MICROGRID OPTIMAL OPERATION

CHEN YUMIN

School of Electrical & Electronic Engineering

A thesis submitted to the Nanyang Technological University
in partial fulfillment of the requirement for the degree of
Master of Engineering

2019

Acknowledgments

Many people have helped me a lot in this thesis writing, including my supervisor, my seniors, my parents, and friends.

Firstly, I would like to express my sincere gratitude to my supervisor, Prof. Xu Yan, for his invaluable instructions and comments, extraordinary patience and consistent encouragement on my research. He gave me much help by providing me suggestions and inspiration for novel ideas. It is his advice that draws my attention to all these new things, like multi-energy microgrid, system operation, stochastic renewable energy resources and so on. Without him, this thesis cannot be accomplished.

Secondly, I would like to give my heartfelt gratitude to Dr. Zhengmao Li, who led me into the world of multi-energy microgrid operation. He guided me in this research area step by step and also devoted much time and patience in answering my questions. I am also greatly indebted to the seniors at the laboratory, who have instructed and helped me a lot in the past year.

Last my thanks would go to my dear parents for their loving considerations and great confidence in me in the last two years. I also owe my sincere gratitude to my friend, Mr. Zhendong Zhou, who gave his help and time in listening to me and help me work out my problems during the difficult periods of the research.

Statement of Originality

I hereby certify that the work embodied in this thesis is the result of original research, is free of plagiarised materials, and has not been submitted for a higher degree to any other University or Institution.

27/103/2019.....

Date

.....Chen Yumin.....

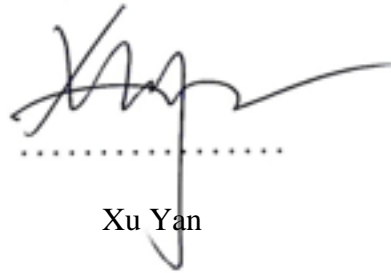
Chen Yumin

Supervisor Declaration Statement

I have reviewed the content and presentation style of this thesis and declare it is free of plagiarism and of sufficient grammatical clarity to be examined. To the best of my knowledge, the research and writing are those of the candidate except as acknowledged in the Author Attribution Statement. I confirm that the investigations were conducted in accord with the ethics policies and integrity standards of Nanyang Technological University and that the research data are presented honestly and without prejudice.

28/03/2019

Date

A handwritten signature in black ink, consisting of stylized, overlapping loops and a long horizontal stroke extending to the right. The signature is written above a dotted line.

Xu Yan

Authorship Attribution Statement

This thesis contains material from 2 papers published in the following peer-reviewed journals / from papers accepted at conferences in which I am listed as an author.

Chapter 4 is published as Y. Chen, Y. Xu, Z. Li, S. Feng, C. Hu, and K. L. Hai, "Optimally Coordinated Operation of a Multi-Energy Microgrid with Coupled Electrical and Heat Networks," in 2018 International Conference on Power System Technology (POWERCON), 2018, pp. 218-224: IEEE.

The contributions of the co-authors are as follows:

- Professor Yan Xu provided the initial project direction and edited the manuscript drafts.
- I prepared the manuscript drafts. The manuscript was revised by Dr Zhengmao Li and Dr Shanqiang Feng.
- I co-designed the study with Professor Yan Xu and performed all the simulation tests at the School of Electrical & Electronics Engineering I also analyzed the simulation results.
- Dr Koh Leong Hai assisted in the collection of the electrical network load, distribution generators data.
- Dr Zhengmao Li assisted in the programming on the General Algebraic Modeling System (GAMS) software.
- Dr Chunchao Hu assisted in the collection and provide guidance in the smart grid area.

Chapter 5 is accepted as Y. Chen, Y. Xu, Z. Li, X. Feng. "Optimally Coordinated Dispatch of Combined-Heat-and-Electrical Network", IET Generation, Transmission & Distribution, 2019.

The contributions of the co-authors are as follows:

- Professor Yan Xu suggested the research topic of this paper and edited the manuscript drafts.
- I wrote the drafts of the manuscript. The manuscript was revised together with Dr Zhengmao Li and Dr Xue Feng.
- I conducted all the simulation tests on 33-bus multi-energy microgrid and 69-bus multi-energy microgrid.
- Dr Zhengmao Li assisted in applying the demand response management (DRM) in microgrid operation problem.

27/03/2019
.....

Date

Chen Yumin
.....

Chen Yumin

Table of Contents

Acknowledgments	i
Abstract.....	ix
List of Figures.....	x
List of Tables	xii
List of Abbreviations	xiii
List of Nomenclature	xiv
Chpater 1 Introduction.....	1
1.1 Background and Motivation.....	1
1.2 Literature Review.....	4
1.3 Major Contributions of the Thesis	6
1.3.1 Comprehensive System-Wide Dispatch Method for MEMG	6
1.3.2 Demand Response Management	7
1.3.3 Specific Model of DHN	7
1.3.4 Two-Stage Optimization Approach.....	8
1.4 Organization of the Thesis	8
Chpater 2 MEMG Modelling.....	10
2.1 Introduction.....	10
2.1.1 Introduction to Microgrid.....	11
2.1.2 Introduction to Multi-Energy Microgrid (MEMG)	11
2.2 Combined Heat and Power (CHP) Plant.....	12
2.3 Electric Boiler (EB)	14
2.4 Photovoltaic Panel (PV).....	15
2.5 Wind Turbine (WT)	16
2.6 Energy Storage (ES)	17
2.7 Summary	19
Chpater 3 District Heat Network (DHN).....	20
3.1 Introduction.....	20
3.2 Introduction to DHN	20
3.3 DHN Modelling	21

3.3.1 Balance of Nodal Flow	21
3.3.2 Temperature Mixing.....	22
3.3.3 Heat Power of Pipe.....	23
3.3.4 Temperature Quasi-Dynamics.....	23
3.3.5 Heat loads.....	26
3.4 Summary	27
Chpater 4 Optimally Coordinated Operation of a MEMG with Coupled Heat and Electrical Networks 28	
4.1 Introduction.....	28
4.2 Model of the Proposed Method.....	29
4.2.1 Objective Function	29
4.2.2 Constraints.....	30
4.2.3 Solution Algorithm.....	32
4.3 Case Studies	33
4.3.1 Tested System	33
4.3.2 Simulation Results.....	37
4.4 Summary	42
Chpater 5 Optimally Coordinated Dispatch of MEMG with Demand Response	43
5.1 Introduction.....	43
5.2 Demand Response Management (DRM)	44
5.2.1 Introduction to DRM.....	44
5.2.2 Price-based Demand Response (PBDR) Modelling.....	46
5.2.3 Indoor Temperature Control (ITC) Modelling	47
5.3 Coordinated Operation Method Considering DRM.....	49
5.3.1 Objective Function	49
5.3.2 Constraints.....	50
5.3.3 Model Linearization	52
5.4 Simulation	53
5.4.1 Tested Systems.....	53
5.4.2 Results and Discussion.....	57
5.5 Summary	61
Chpater 6 Two-Stage Stochastic Operation of MEMG	63
6.1 Introduction.....	63
6.2 Modelling of Uncertainties	64
6.2.1 Scenario Construction	64
6.2.2 Scenario Reduction	65
6.3 Two-Stage Optimization Approach	65

6.4 Simulation and Discussion.....	67
6.4.1 Tested System	67
6.4.2 Simulation Results.....	69
6.5 Summary	72
Chapter 7 Conclusions and Future Works	74
7.1 Conclusions.....	74
7.2 Future Works.....	75
Author's Publication.....	77
Reference	78

Abstract

With the increasing demand for global energy, multi-energy microgrids have drawn more attention in recent years. In a multi-energy microgrid (MEMG), different kinds of energies like heat, electricity, cooling, and gas are interacted with each at various levels, aiming to increase the overall energy utilization efficiency. MEMG usually contains many different generation units and ancillary components like combined heat and power (CHP) plant, photovoltaic cell (PV), wind turbine (WT), electric boiler (EB), fuel cell (FC), energy storage (ES) and so on. Since the operational properties and technical limits are quite different, how to optimally dispatch these units is a key research topic in this area.

Besides, the properties of these energy networks are also different. For instance, we usually assume that electricity can be delivered to customers immediately without any time delay. However, in the heat network, thermal energy is transferred by hot water in pipes. Since the flow rate of hot water is much slower than the transmission speed of electricity, there is a transmission delay ranging from minutes to hours in the heat network. Thus, it is valuable to consider the transferring time delay in MEMG. What's more, the uncertainties of renewable energy resources pose a significant challenge to the operation of MEMG.

The focus of this research topic is to propose a suitable coordinated operation method for MEMG with coupled heat and electrical networks, in which the specific models of electrical network and heat network are systematically studied. Further, demand response management (DRM) and the randomness of renewable energy resources are considered in the proposed method to better operate MEMG.

All the proposed operation and planning methods have been verified in simulation using GAMS and HOMER. The proposed method is simulated on a MEMG with coupled heat and electrical network, which is based on the IEEE 33-bus radial distribution network and a 13-pipe DHN.

List of Figures

Figure 1-1. Power shortage in Pakistan (Energy Crisis in Pakistan: The Challenges and Alternatives. [Online]. Available: http://www.pakistanreview.com)	1
Figure 1-2. A typical structure of MEMG with coupled heat and electrical network. ...	3
Figure 1-3. Properties of different energy networks.....	3
Figure 2-1. Typical structure of MEMG.....	11
Figure 2-2. Working flow of CHP plant.	13
Figure 2-3. Power output of wind turbine under different wind speed	16
Figure 3-1. Schematic diagram of DHN.....	21
Figure 3-2. Water mass flowing in heat pipes.	22
Figure 3-3. Vertical section of a heat pipe.....	24
Figure 4-1. Schematic diagram of the tested MEMG.....	33
Figure 4-2. Predicted weather condition data over 24 hours.	34
Figure 4-3. Electricity price of the whole day.	34
Figure 4-4. Power balance conditions. Case1 (a), Case2 (b), Case3 (c).....	38
Figure 4-5. Heat conditions. Case1 (a), Case2 (b), Case3 (c).....	40
Figure 4-6. Heat generated by CHP and EB in the three cases.	41
Figure 4-7. Storage status of heat network of 24 hours under Case3.	41
Figure 5-1. Heat conduction through building shells.	48
Figure 5-2. Flowchart of the proposed method.	53

Figure 5-3. Schematic diagram of 33-bus MEMG.	54
Figure 5-4. Day-ahead 24h power transaction price.....	55
Figure 5-5. Schematic diagram of 69-bus MEMG.	56
Figure 5-6. Electric load profile.....	58
Figure 5-7. Power balance in 33-bus MEMG. (a) Case1. (b) Case2. (c) Case3.....	58
Figure 5-8. Simulation Results of Heat Power.	59
Figure 5-9. Power balance in 69-bus MEMG. (a) Case1. (b) Case2. (c) Case3.....	61
Figure 6-1. Flow chart of two-stage optimization approach.....	66
Figure 6-2. Flow chart of two-stage optimization approach.....	68
Figure 6-3. Charging/discharging power of (a) EES. (b)HST.....	70
Figure 6-4. Specified input data for second stage. (a)Load. (b) RES generation. (c) Electricity price.....	71
Figure 6-5. Operation results in the second stage. (a) Electricity balance condition. (b)Heat condition.	72

List of Tables

Table 4-1. System parameters.....	34
Table 4-2. Parameters of working units in MEMG	34
Table 4-3. Heat pipe parameters	35
Table 4-4. DHN parameters.....	35
Table 4-5. Parameters of EES [7]	35
Table 4-6. Mass flow rate of each pipe.....	35
Table 4-7. Impedance of each bus [34]	35
Table 4-8. Cases summary	37
Table 4-9. Simulation results	41
Table 5-1. Simulation results	46
Table 5-2. Location of each unit in 33-bus MEMG	54
Table 5-3. EES Parameters	55
Table 5-4. DHN Parameters	55
Table 5-5. Units Parameters	56
Table 5-6. Configuration of the tested systems	57
Table 5-7. Total costs in 69-bus system	61
Table 6-1. Parameters of units	68
Table 6-2. Unit commitment results	69
Table 6-3. Total cost and voltage violation	72

List of Abbreviations

MEMG	Multi-Energy Microgrid
CHP	Combined Heat and Power
DHN	District Heat Network
DRM	Demand Response Management
PV	Photovoltaic Cell
WT	Wind Turbine
EB	Electric Boiler
ES	Energy Storage
DG	Distributed Generator
DHN	District Heat Network
PBDR	Price-Based Demand Response
ITC	Indoor Temperature control
O&M	Operation & Maintenance
CU	Controllable Unit
UU	Uncontrollable Unit
MT	Micro Turbine
EES	Electrical Energy Storage
HST	Heat Storage Tank
MILP	Mix-Integer Linear Programming

List of Nomenclature

Chapter 2-4

Sets and Indices

t/T	Index/sets of all periods.
B, b	Set/Index of buildings (heat loads) in DHN.
J, j	Set/Index of PBDR levels.
I, i	Set/Index of nodes in the electrical network.
N_{ps}/N_{pr}	Sets of connection nodes in the supply/return network.
K_{hs}/K_{hl}	Sets of pipes connected to heat sources/heat loads.
K_{ps}/K_{pr}	Sets of all pipes in the supply/return network.
$K_{n,s}^+/K_{n,s}^-$	Sets of all pipes starting/ending at node n in the supply network.
$K_{n,r}^+/K_{n,r}^-$	Sets of all pipes starting/ending at node n in return network.
n/N	Index/sets of all nodes in the heat network.
k/K	Index/sets of all pipes in the heat network.
l/L	Index/sets of heat loads in the heat network.
u/U	Index/sets of all the units in MEMG.

Variables

$Q_{CHP-ex,t}$	Exhaust heat of CHP plant at period t , kW.
$Q_{CHP,t}/P_{CHP,t}$	Heat/electric power output of the CHP plant at time t , kW.
$C_{CHP,t}^f$	Fuel cost of CHP plant at period t , ¥.
$Q_{EB,t}$	Heat power produced by EB at period t , kW.
$P_{WT,t}, P_{PV,t}, P_{CHP,t}$	Electric power of WT/PV/CHP at period t , kW.
$P_{EB,t}$	Electric power consumed by EB at period t , kW.
v_t	Ambient wind speed at period t , m/s.
$C_{WT}^m, C_{PV}^m, C_{CHP}^m$	Unit O&M price of WT/PV/CHP, ¥/kW.
$C_{EB}^m, C_{EES}^m, C_{HES}^m$	Unit O&M price of EB/EES/HES, ¥/kW.
$C_{WT}^{cap}, C_{PV}^{cap}, C_{CHP}^{cap}$	Capital cost of WT/PV/CHP, ¥.
$C_{EB}^{cap}, C_{EES}^{cap}, C_{HES}^{cap}$	Capital cost of EB/EES/HES, ¥.
$E_{EES,t}$	Energy content of EES at time t , kWh.
$H_{HES,t}$	Thermal energy content of HES at time t , kWh.
$P_{EES,t}^{ch}, P_{EES,t}^{dis}$	Charging/discharging power of EES at time t , kW.
$P_{HES,t}^{ch}, P_{HES,t}^{dis}$	Charging/discharging power of HES at time t , kW.
$U_{EES,t}^{ch}/U_{EES,t}^{dis}$	Binary state variables with $U_{EES,t}^{ch} = 1/U_{EES,t}^{dis} = 1$, EES is charging/discharging
$U_{HES,t}^{ch}/U_{HES,t}^{dis}$	Binary state variables with $U_{HES,t}^{ch} = 1/U_{HES,t}^{dis} = 1$ HES is charging/discharging
$m_{s,k,t}/m_{r,k,t}$	Mass flow rate of pipe k at period t in the supply/return network, kg/h.
$Q_{s,k,t}^+/Q_{s,k,t}^-$	Heat power at the starting/ending point of pipe k in supply network at period t , kW.

$Q_{r,k,t}^+ / Q_{r,k,t}^-$	Heat power at the starting/ending point of pipe k in return network at period t , kW.
$T_{s,n,t} / T_{r,n,t}$	Temperature at node n in the supply/return network at time t , °C.
$T_{s,k,t}^+ / T_{s,k,t}^-$	Temperature at the starting/ending point of pipe k in supply network at time t , °C.
$T_{n,s}^m / T_{n,r}^m$	Mixed temperature at node n of supply/return network at time t , °C.
$\mu_{k,t}$	Heat power loss per unit length of pipe k , kW/km.
$T_{k,t}^{avg}$	Average temperature of pipe k , °C.
$T_{am,t}$	Ambient temperature at period t , °C.
C_{total}	Net operating cost of MEMG, ¥.
C_{CP}	Average daily capital cost, ¥.
$C_{f,t}, C_{om,t}$	Fuel cost/ Operation & maintenance (O&M) cost at time t , ¥.
C_n	Average daily cost of laying heat pipes, ¥.
$H_{load,i,t}$	Heat load of building l at period t , kW.
$\psi_{k,t} / \phi_{k,t}$	Numbers of periods representing time delays of temperature changes in pipe k at time t .
$R_{k,t} / S_{k,t}$	Coefficient variables of pipe k at period t related to the previous mass flow.
$K_{k,t,\omega}$	The ω -th coefficient variable defining the temperature at the ending point of pipe k at time t .
$J_{k,t}$	Temperature drop coefficient of pipe k at period t .
$P_{load,i,t}, Q_{load,i,t}$	Active/reactive power at node i with PBDR strategy.
$P_{load,i,t}^o, Q_{load,i,t}^o$	Original active/reactive power at node i without PBDR strategy.
$H_{b,t}^T$	Heat conduction power of building b .
$H_{b,t}^{load}$	Design heat load of building b at time t .
$H_{s,b,t}^T$	Heat energy conduction through building shells of building b .
$T_{in,b,t}$	Indoor temperature of building b .
$U_{CHP,t}^i, U_{EB,t}^i$	On-off status of CHP, electric boiler at time period t .
$P_{gd,t}, P_{sd,t}$	Power purchasing from/selling to the utility grid at time t .
$P_{i,t}, Q_{i,t}$	Active/reactive power flow between node i and $i+1$ during time period t .

Parameters

η_L	Loss rate of heat dissipation.
η_{CHP}	Electrical efficiency of CHP.
C_{OPh}	Performance coefficient of absorption chiller.
η_h	Recovery rate of absorption chiller.
C_{CH4}	Unit price of natural gas, ¥/kWh.
L_{HVG}	Low calorific value of natural gas.
$\lambda_1, \lambda_2, \lambda_3$	The power coefficient of WT.
$P_{r,WT}$	Rated output power of WT, kW.
$C_{WT}^m, C_{PV}^m, C_{CHP}^m$	Unit O&M price of WT/PV/CHP, ¥/kW.

C_{EB}^m, C_{EES}^m	Unit O&M price of EB/EES, ¥/kW.
$C_{WT,u}^{cap}, C_{PV,u}^{cap}, C_{CHP,u}^{cap}$	Unit capital price of WT/PV/CHP, ¥/kW.
$C_{EB,u}^{cap}, C_{EES,u}^{cap}$	Unit capital price of EB/EES, ¥/kW.
$G_{T,t}$	The solar radiation incident on the PV array in the current time step, kW/m ² ,
$\overline{G_{T,STC}}$	The incident solar radiation at standard test conditions, kW/m ² .
v_{ci}, v_{co}, v_{rate}	Cut-in wind speed, cut-out wind speed, rated wind speed at time t , m/s.
f_{pv}	The PV derating factor.
α	The EES decay rate.
β	The HST decay rate.
η_{ch}, η_{dis}	Charging/discharging efficiency of EES.
$\lambda_{ch}, \lambda_{dis}$	Charging/discharging efficiency of HST.
δ_j	Load demand response level j .
ε	Price elasticity of electric demand.
B	Price-based demand response constant.
$C_{pr,t}$	Price of exchange power with the utility grid.
l_j^{level}	Load demand response rate of level j .
$T_{am,t}$	Outdoor temperature at time period t .
R_T	Heat resistance of building shells.
τ	Coefficient of heat conduction.
C_{air}	Specific heat capacity of air.
η_{ra}	Efficiency of radiator.
$P_{max}, Q_{max},$	maximum active/reactive power of a branch.
T_s^{min}, T_s^{max}	Minimum/maximum temperature of water flowing in supply pipes.
T_r^{min}, T_r^{max}	Minimum/maximum temperature of water flowing in return pipes.

Chapter 5

Sets and Indices

I, i	Set/Index of buses.
J, j	Set/Index of PBDR price levels.
K, k	Set/Index of thermal zones.
G, g	Set/Index of controllable generators/auxiliary units.
T, t	Set/Index of time periods.

Parameters

$\lambda_1/\lambda_2/\lambda_3$	Coefficient of the wind turbine.
η_L	Loss rate of heat dissipation.
η_{CHP}	Electrical efficiency of CHP.
C_{OPh}	Performance coefficient of absorption chiller.
C_{gas}	Unit price of natural gas, ¥/kWh.
L_{HVNG}	Low calorific value of natural gas.
$P_{r,WT}$	Rated output power of WT, kW.
C_g^{OM}	Unit O&M price of component g , ¥/kW.
C_g^{SU}	Unit Start-up cost of component g , ¥.
$C_{EES}^{OM}/C_{HST}^{OM}$	Unit O&M price of EES/HST, ¥/kW.
C_g^{SD}	Unit shut-down cost of component g , ¥.
V_0	Voltage of substation, normally 1 p.u.
R_i, X_i	Impedance of branch from bus i , p.u.
P_{max}/P_{min}	Maximum/minimum power of the branch from bus i , kW.
ΔV_{max}	Allowed mismatch range of voltage at bus i , p.u.
V_0	Voltage of substation, p.u.
p_g^{MAX}/p_g^{MIN}	Maximum/minimum power of unit g , kW.
$p_{EES,t}^{dmax}/p_{EES,t}^{cmax}$	Maximum discharging/charging power of EES, kW.
$\mu_{EES}^{MIN}/\mu_{EES}^{MAX}$	Minimum/maximum state of charge of EES.

Variables

$Q_{CHP-ex,t}$	Exhaust heat of CHP plant at period t , kW.
$Q_{CHP,t}/P_{CHP,t}$	Heat power output/electric power output of CHP plant at period t , kW.
$\eta_{CHP,t}$	Electrical efficiency of CHP at period t .
$C_{CHP,t}^f$	Fuel cost of CHP plant at period t , ¥.
$Q_{EB,t}/P_{EB,t}$	Heat/ electric power produced by EB at period t , kW.
$P_{WT,t}, P_{PV,t}$	Electric power output of WT/PV at period t , kW.
v_t	Ambient wind speed at time t , m/s.
$C_{g,t}^{OM}$	O&M cost of component g at time t , ¥.
$C_{g,t}^{SU}$	Start-up cost of component g at time t , ¥.

$C_{g,t}^{SD}$	Shut-down cost of component g at time t , ¥.
$C_{EES,t}^{OM}/C_{HST}^{OM}$	O&M cost of EES/HST at time t , ¥.
$U_{g,t}^i$	Binary state variables with $U_{g,t}^i = 1$, component g at bus i is operating.
$C_{ex,t}$	Power exchange cost at period t , ¥.
$E_{EES,t}$	Energy content of EES at time t , kWh.
$P_{EES,t}^{ch}/P_{EES,t}^{dis}$	The charging/discharging power of EES at time t , kW
$U_{EES,t}^{ch}/U_{EES,t}^{dis}$	Binary state variables with $U_{EES,t}^{ch} = 1/U_{EES,t}^{dis} = 1$, EES is charging/discharging
$H_{HST,t}$	Energy content of HST at time t , kWh.
$Q_{HST,t}^{ch}/Q_{HST,t}^{dis}$	The charging/discharging heat power of EES at time t , kW
$V_{i,t}$	Voltage of bus i (p.u.).
$P_{gd,t}, P_{sd,t}$	Electricity bought from/ sell to the utility grid at period t , kW.
$P_{i,t}/Q_{i,t}$	Active/reactive power flow between node i and $i+1$, p.u.
$P_{load,i,t}/Q_{load,i,t}$	Active/reactive load at node i during period t , p.u.
$P_{g,t}^i$	Power of unit g at bus i during period t , kW.

Chapter 1 Introduction

1.1 Background and Motivation

Since the mid-1960s, the world has suffered from various energy crises. Some countries are facing severe energy shortages these years. For instance, Pakistan has lacked the energy it needs for almost a decade [1]. Producers and consumers around the country are facing a power shortage of up to 12 hours per day.



Figure 1-1. Power shortage in Pakistan (Energy Crisis in Pakistan: The Challenges and Alternatives. [Online]. Available: <http://www.pakistanreview.com>)

Although many nations and countries are actively putting efforts to decrease their dependence on fossil fuels, our demand for global energy is still significantly rising year by year. It is revealed in The 2017 Global Energy and CO₂ Status Report that last year, our global energy demand increased by 2.1%, which is more than twice as the increase in 2016. Further, it is estimated by some scientists and researchers that fossil fuels may run out around the 2080s. And once they are gone, they will not be reproduced.

Thus, it is a practical need to find solutions to alleviate the severe energy crisis. One possible way is to reduce the dependence of fossil fuels and move forwards to renewable energy resources (RES) like wind power and solar power. Another way is to reduce energy wastage as much as possible and also increase the overall energy utilization efficiency. However, in a conventional power system, different energy sectors are produced and consumed separately without any interaction [2]. For instance, we usually depend on generators to produce electricity, and we burn fuels through boilers to supply thermal energy. Traditionally, there is no interaction between heat and electricity. This kind of energy system can only achieve 45% energy utilization efficiency.

However, the interactions between different energy sectors have already taken place and are dramatically increasing. For example, heat, cooling, gas, and electricity are interacted with each other through many distributed technologies, like CHP plant, EB, electric heat pump and so on. Similarly, transportation network and electrical network can be integrated together by means of electric vehicle (EV).

In this outlook, one key aspect to evolve towards a cleaner and more affordable energy system is to develop MEMG, in which various energy sectors are integrated together, aiming to enhance the energy utilization efficiency and system economic benefits. Fig. 1-2 shows a typical structure of MEMG with coupled heat and electrical network, whereas the red part denotes heat network and the blue part denotes electrical network. It can be seen that there are usually many different units in a MEMG, like the wind turbines, photovoltaic cells, energy storage, electric boiler, and so on. Since the operational characteristic of them are quite different, how to optimally schedule them based on their own properties is a key research topic in this area.

What's more, the properties of these energy networks are also different, which can be found in Fig. 1-3. Unlike other forms of energy, electricity is not easily stored abundantly and thus must generally be used as it is generated. Besides, since electricity can be

transferred much faster than gas and heat, it is thought to be low inertia. And the power system needs to be resilient and stable to supply reliable electricity to customers. However, in DHN, the thermal output at a certain time is, in fact, responsible for heat demand several hours later owing to the transmission delay. Besides, the indoor temperature decreases slowly when heating stops due to the thermal inertia of maintenance structure, which leads to high inertia and great loss property of the heat network. Based on the above analysis, the properties of electricity, heat, and other kinds of energy networks are quite different. In this light, how to integrate them based on their own properties has also captured a large amount of researchers' attention in recent years.

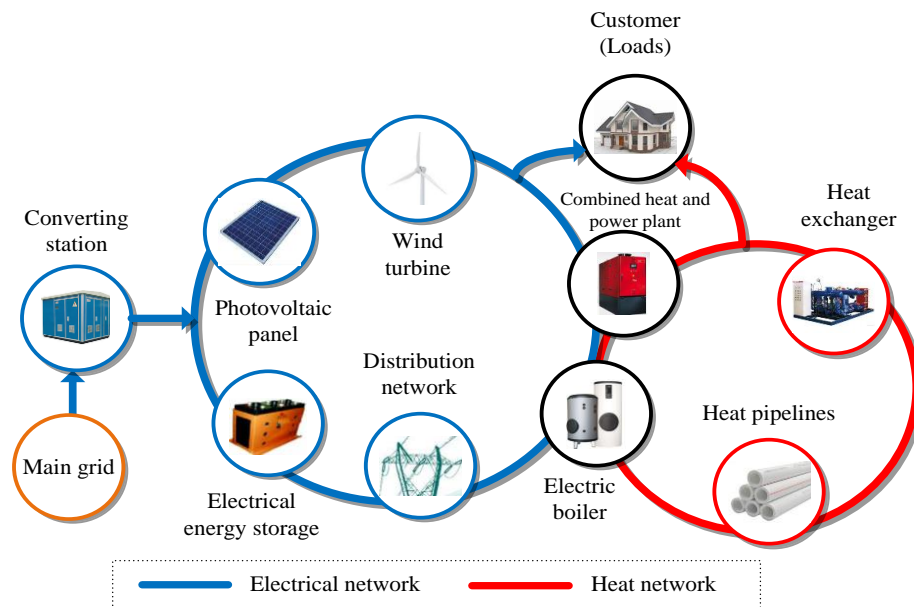


Figure 1-2. A typical structure of MEMG with coupled heat and electrical network.

Electrical network	Heat network	Transportation network
<ul style="list-style-type: none"> • Low inertia • Not be stored abundantly • Resilient 	<ul style="list-style-type: none"> • High inertia • Transmission delay • Great loss 	<ul style="list-style-type: none"> • Medium inertia • Resilient

Figure 1-3. Properties of different energy networks.

1.2 Literature Review

Although many studies have been done on the optimal operation of MEMG with coupled heat and electrical network, some issues remain open. With regard to multi-energy integration (mainly heat and power), reference [3] proposes a hybrid method to minimize excess electrical and heat energy generated by CHP units. In [4], following heat load (FHL) and following electric load (FEL) operating strategies for CHP plants are compared. Similarly, another study [5] introduces an improved operating strategy for CHP units under different operation logics. The study in [6] uses a comprehensive methodology to optimally control the operation of lead-acid batteries under a real-time pricing scheme, aiming to minimize the net operating cost. These researches are proved to be effective and indeed increased the overall system utilization efficiency and economic benefits, but they only investigate on the operation of just one generator/auxiliary unit in MEMG (e.g., CHP plant, ES, heat pump), their coordination with other distributed generators (DGs) from a system perspective is seldom studied.

Besides, some studies have investigated the coordinated system dispatch strategy of microgrids at system levels. Li [7] proposes a comprehensive optimal coordination energy scheduling method for MEMG throughout a system under both grid-connected and islanded modes. Reference [8] utilizes a robust optimization method to optimally operate MEMG, considering the flexibility of heat and electrical loads and the uncertainties of renewable energy resources. Apart from that, other studies [9-11] also put efforts on this topic, but most of the current researches only focus on the models of only one kind of energy, such as power flow balance, voltage or phase angle constraints of electrical networks, while little emphasis is placed on the topology and specific models of heat networks. As mentioned before, when we are looking into the multi-energy system, the properties of different energy networks should be taken into consideration. Thus, the aforementioned studies may not be practical enough for real-life applications.

Currently, the district heat network (DHN) is getting more and more popular all over the world, for its benefits of reducing the use of fossil fuels and thermal energy transmission loss. Several researches have been done on the operation of coupled heat and electrical network [12-14] with a specific mathematical model of DHN. Li [12] proposes a two-stage method to calculate the temperature at the ending point of each pipe so that the transmission delay and the high-inertia property of the heat network can be fully considered. In his paper, a preliminary investigation has been carried out on the storage potential of DHN. What's more, another study [14] also introduces an optimal operation model of integrated heat and electrical network, which considers the dynamic characteristics of DHN. The simulation results show that similar to DHN, thermal buildings can be seen as thermal storage units with higher economic benefits. Nevertheless, these works only focus on the model of heat networks, and only considers the power balance equation for the electrical network in their model. Besides, the coordination between heat networks and power networks is not systematically investigated in these researches works. Further, few of them consider heat storage potential of DHN due to high inertia of internal flowing hot water, i.e., mass flow rate of hot water is not fast enough and heat generation in DHN is usually consumed several time periods later. With the inertia property, the heat network can be seen as a buffer that stores/releases heat energy. That said, it is necessary to study the dynamic characteristics of the DHN, while taking into account its coordination with the power network.

For the moment, it is very hard to forecast the generation output of renewable generators (WTs, PVs) due to their stochastic properties, which poses a significant challenge to the operation of MEMG [8]. Most of the above studies assume an accurate forecast of renewables, i.e., the generation outputs of WTs and PVs are inputs, not unknown variables. Nevertheless, these uncertainties will have negative effects on the robustness of MEMG operation, which cannot be ignored. It is revealed in [15] that the operation the larger of forecast error of uncertain renewables, the higher of the MEMG's operation

risk level. To address this problem, literature [16] proposes a stochastic game approach to optimize the MEMG operation, in which the uncertainty samples are selected randomly. To solve this problem, Wang et al [17] employ prediction errors to optimize the system operating cost and reserve capacity. The prediction errors are randomly generated to simulate the stochastic variation of RES. Besides, [18] proposes a two-stage stochastic approach for power production and trading in the microgrid. Reference [19] also employs a chance-constrained two-stage stochastic optimization method to handle the uncertainties from wind output. The above papers verify that the stochastic optimization method is effective in smoothing out the fluctuations from RES [20]. Nevertheless, they are more focusing on the electrical network. Little attention is paid to the uncertainties in MEMG.

What's more, with the increase in population, electrical loads and thermal loads are growing dramatically year by year. The ever-growing customer's demands may cause a severe imbalance between generation and consumption because the installed capacity of generators is limited. Demand response management (DRM) is an effective approach to alleviate this problem and it has already been used to reshape the load profile recently. The ongoing research on the DRM [21, 22] shows that day-ahead DRM can effectively solve the mismatch problem between supply and demand, as well as increase the system's economic performance. However, the DSM is rarely considered in the coupling energy networks.

1.3 Major Contributions of the Thesis

Main contributions are explained as follows:

1.3.1 Comprehensive System-Wide Dispatch Method for MEMG

A comprehensive system-wide dispatch method for the coupled heat-and-electrical network is developed. While most of the current researches on multi-energy microgrid

only focuses on the dispatch of one key unit (like CHP plant, ES, heat storage tank) or single-energy network, this thesis aims to optimally coordinate all the controllable units in MEMG. More importantly, in the proposed dispatch model, not only the operating constraints of power network (power flow balance, voltage constraints as well as some output limits, ramp up/down limits of components and so on) are taken into account, a detailed model of heat network has also been built and coupled with the power network. Simulation results show that the heat network and power network can be strongly integrated with each other at a system level through this method.

1.3.2 Demand Response Management

Price-based demand response (PBDR) and Indoor temperature control (ITC) strategies are employed to make heat and electrical loads flexible so that overall economic benefits and flexibility of units dispatching can be markedly improved. Demand response strategies (especially the thermal demand response) are rarely considered in MEMG operation. With the development of the smart grid, demand response management will become more and more popular, simulation results can provide some valuable instructions for future day-ahead operation problems.

1.3.3 Specific Model of DHN

Most of the existing works about MEMG operation did not consider the topology and specific model of the heat network, and they usually assume that heat energy can be transferred to customers immediately without any time delays, just like an electrical network, which is not practical. In this thesis, a new and comprehensive heat network model is proposed, which fully considers the transmission delays, mixing temperature and dynamic mass flow. Apart from that, most of the existing works did not consider the potential thermal storage capability of a DHN, in this thesis, DHN is utilized as a heat storage tank (HST) to make the system operation more flexible and economical.

1.3.4 Two-Stage Optimization Approach

A two-stage stochastic optimization method is presented to consider the varied randomness in MEMG: the on/off statuses of each unit and charging/ discharging power of ESs are optimized in the day-ahead stage since they need to be decided under uncertainties in advance. The power outputs of each generator are optimized in the intra-day stage, which acts as a recourse to complete the operational decisions.

1.4 Organization of the Thesis

The following of the thesis is organized as follows:

Chapter 2 introduces the basic structure of MEMG with coupled heat and electrical networks. Then, the mathematical model of each working unit in MEMG is presented, in which the external characteristics and economic items are formulated and summarized.

Chapter 3 introduces the topology of DHN and then proposes a comprehensive model of it. The nodal balance flow constraints, mixing temperature equations, hydraulic balance, dynamic heat loss as well as transmission delay are investigated.

In **Chapter 4**, a system-wide optimal coordinated operation method for a MEMG with coupled heat and electrical networks is proposed. In this method, both electric power flow and district heat network (DHN) constraints are taken into consideration. In order to increase the overall economic benefits and dispatch flexibility, DHN is utilized as a heat storage tank to store/release heat energy. Further, three case studies are designed and simulated to show the effectiveness and benefits of the proposed approach.

Chapter 5 presents a system-wide coordinated operation approach for MEMGs, which aims to schedule different components including generation resources and flexible loads.

In this approach, the coupling constraints of electrical and heat network, dynamic characteristics of heat network as well as the power flow constraints are comprehensively modeled. Besides, demand response management is employed for more flexible operation of the combined electrical and thermal network.

Chapter 6 proposes a two-stage stochastic dispatch method to optimally schedule the working units in MEMG under varied uncertainties from RES, electricity price and loads. In this method, the charging/discharging power of energy storages (including thermal storage and electrical energy storage) as well as on/off status of generators are scheduled in the day-ahead stage; in the intra-day stage, the output power of generation units and auxiliary units will be optimized to act as a supplement. Finally, simulation results demonstrate that the two-stage stochastic optimization method can markedly reduce total operating costs and make the system more robust.

Chapter 7 concludes the whole thesis and talks about some questions that are of great interest to future research studies in this area.

Chapter 2 MEMG Modelling

2.1 Introduction

Compared to conventional large grid, microgrid is an independent entity, which can interconnect with the main grid through a converting switch. Different kinds of DGs are often integrated into a microgrid. Different from traditional centralized generation technology, the microgrid provides the benefits of rich transmission resources, low control, and operational cost as well as little transmission loss. In the meantime, DG can help to do peak load shifting and can markedly enhance the reliability of power supply. Hence, the DG technique is widely utilized as an effective support and supplement in MEMG. Common DGs mainly contain microturbine, diesel generator, fuel cell, wind turbine, photovoltaic panel and so on.

However, with the development of research for the DG technique, problems like high access cost, difficult to control have gradually emerged. In order to solve these problems, microgrid technology arises at the time requires. Microgrid technique can effectively integrate the benefits of DG, and also provide a new technical way for large scale application of grid-connected generation of RES [21]. For the utility grid, a microgrid can be seen as a normal dispatchable unit; for consumers, microgrid functions as a controllable energy source, which can satisfy the diverse requirements from end-users. Since microgrid is beneficial for creating a favorable environment of utilizing renewable energy resources, it is valuable for us to put effort into investigating it.

This chapter aims at introducing microgrid and MEMG. Besides, the mathematical models of different units in MEMG are also presented.

2.1.1 Introduction to Microgrid

A microgrid is a small size grid in which a group of localized power generation (especially RES generation) and loads are employed. It can operate in the grid-connected mode to exchange electric power with the utility grid, but can also disconnect to islanded mode—and work as an independent entity.

There are four key components in a microgrid: local generation, consumption, energy storage as well as point of coupling (PCC).

2.1.2 Introduction to Multi-Energy Microgrid (MEMG)

To alleviate the serious worldwide energy crisis, traditional microgrid evolves towards to multi-energy microgrid (MEMG) for higher energy utilization efficiency. A very essential topic is to provide multiple end-use demands such as heating, cooling, and electricity simultaneously since this allows energy carrier substitution waste heat utilization.

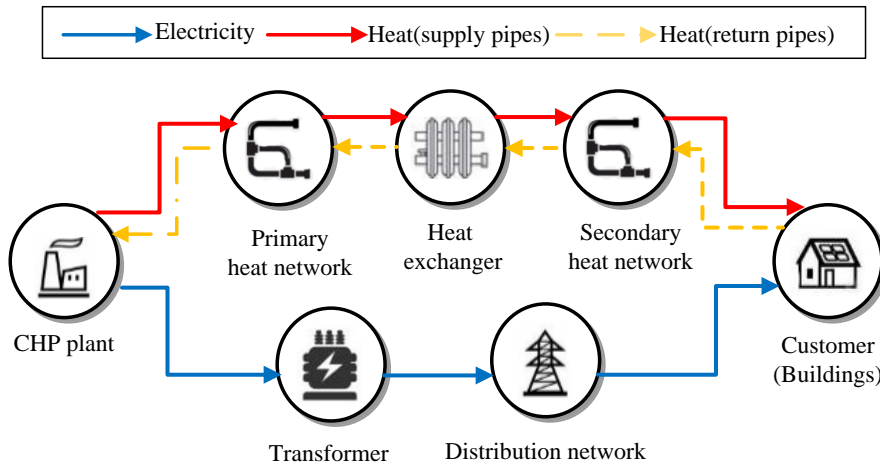


Figure 2-1. Typical structure of MEMG.

Fig.2-1 shows the typical structure of a MEMG with coupled heat and electrical networks. It can be found in the figure that there are two kinds of energy flows in this MEMG. The blue part denotes an electrical energy network whereas the red/orange part denotes DHN.

Different kinds of working units including combined heat and power (CHP) plants, wind turbines, photovoltaic cells, energy storage (ES) and electric boilers are deployed in this MEMG.

Since we are investigating the operation problem of MEMG, models mainly focus on external characteristics and economic items of each unit [7], i.e., their ON/OFF statuses, generation outputs and operation & maintenance (O&M) cost, fuel cost, etc. The specific models are given in the following contents. It is worth to mention that although internal characteristics may have effects on the operation of the working unit. However, this thesis focuses on the whole system and network-level coordinated dispatch of electricity and heat, therefore internal characteristics can be neglected in the modeling part. Apart from that, since the sizes of CCHP plant, EB, as well as ES are relatively small and they can be flexibly controlled, hence, these working units can be categorized as the controllable units (CU) [7]. On the other hand, due to the random property of RES, generation outputs of renewable generators like WT and PV are uncertain, thus they are regarded as uncontrollable units (UU). The mathematical model of units in an electrical network can be formulated as follows.

2.2 Combined Heat and Power (CHP) Plant

CHP plant has the ability to generate power and heat power at the same time, thus it becomes the core unit in solving the problem of low energy utilization efficiency in separation production problems [4]. A CHP unit usually consists of two main components: microturbine (MT) as well as heat recovery unit. Fig. 2-2 shows the working flow of the CHP plant. The high-level heat energy generated from burning natural gas drives MT to generate power and the waste heat will then be absorbed for supplying heat energy. In this thesis, the Capstone's MT C65 is selected as a representative of the CHP plant.

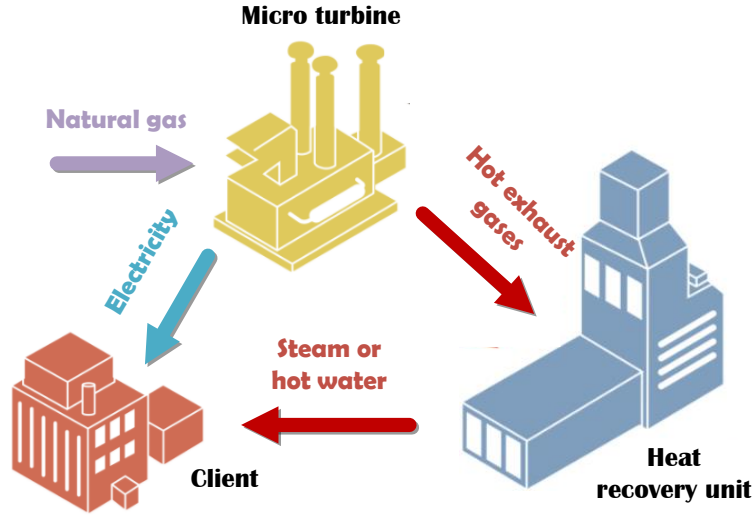


Figure 2-2. Working flow of CHP plant.

Previous research works show that environmental factors like temperature and solar radiation have little effects on the operational status and condition, thus they can be neglected in the mathematical models [3].

The heat output of the CHP plant can be modeled as follows:

$$Q_{CHP-ex,t} = \frac{P_{CHP,t} - \eta_{CHP,t} P_{CHP,t} - \eta_L}{\eta_{CHP,t}} \quad (2.1)$$

$$Q_{CHP,t} = \eta_h C_{OPh} Q_{CHP-ex,t} \quad (2.2)$$

As stated by reference [23], the efficiency of the CHP plant is related to its electric power output at that time, which can be formulated as follow:

$$\eta_{CHP,t} = 0.076 \left(P_{CHP,t} / 65 \right)^3 - 0.31 \left(P_{CHP,t} / 65 \right)^2 + 0.415 \left(P_{CHP,t} / 65 \right) + 0.107 \quad (2.3)$$

In practical power and heating engineering area, the electrical efficiency of the CHP plant has slight fluctuation, thus it is usually assumed that $\eta_{CHP,t}$ is a constant for convenience[7].

The fuel costs of CHP plant at time t can be formulated as:

$$C_{CHP,t}^f = C_{CH4} \frac{P_{CHP,t} \cdot \Delta t}{\eta_{CHP,t} \cdot L_{HVNG}} \quad (2.4)$$

Besides, capital costs and O&M cost of it can be modeled as:

$$C_{CHP}^{cap} = P_{CHP}^{cap} C_{CHP,u}^{cap} \quad (2.5)$$

$$C_{CHP,t}^m = C_{CHP}^m P_{CHP,t} \quad (2.6)$$

Since the waste thermal energy can be reutilized by the CHP system, the overall energy utilization efficiency can be significantly increased. While the traditional method of separate generation has a typical combined efficiency of 44%, CHP plants can achieve at levels as high as 80%.

2.3 Electric Boiler (EB)

EB is a kind of engine that uses electric power to boiler water, thus thermal energy can be generated. EB can be simply installed, flexibly controlled and easily maintained, thus it is receiving wide use in a microgrid for satisfying the thermal requirements. With the help of real-time electricity prices, EB can coordinate with the CHP system to increase the electrical consumption in valley periods. Hence, introducing EB into MEMG can achieve flexible heat-electricity conversion and help to transfer thermal/electric demands from peak to valley periods.

The mathematical model of EB which consumes electricity to produce heat can be formulated as follows. Besides, its O&M costs, as well as capital costs, are presented in (2.8) and (2.9).

$$Q_{EB,t} = P_{EB,t} \eta_{EB} \quad (2.7)$$

$$C_{EB,t}^m = C_{EB}^m P_{EB,t} \quad (2.8)$$

$$C_{EB}^{cap} = P_{EB}^{cap} C_{EB,u}^{cap} \quad (2.9)$$

2.4 Photovoltaic Panel (PV)

Since solar energy is inexhaustible in supply and pollution-free, it has a promising future and is expected to take the place of fossil fuels gradually. The worldwide development of solar energy is extremely dynamic and varies strongly among countries. It is revealed by some reports that worldwide solar installed capacity increased by more than 75 GW and reached at least 303 GW by the end of 2016. China, the United States, and India have the highest installed capacity [24]. Besides, there are more than 20 countries all over the world with PV installed capacity of more than 1GW.

Photovoltaic generation has the ability to convert sunlight directly into electricity through solar panels (usually installed on rooftops), photovoltaic cells or other kinds of engines. Solar power has a lot of advantages: For instance, it is environmentally friendly and would not cause any greenhouse gas after installation. Besides, it can reduce our dependence on fossil fuels. From an economic point of view, a photovoltaic panel can last over 25 years, thus its replacement costs can be extremely low. Currently, photovoltaic generation is a mature technique and it can provide reliable electricity to consumers. However, its drawbacks like low generation efficiency and high generation cost seriously restricted the development.

Because the generation output power of PV is strongly related to surrounding weather conditions, ambient temperature as well as solar irradiation, it is valuable for us to investigate the random distribution of PV power output.

The power output of PV can be modeled as follow. Here, the ITEK's energy SE module PV panel is selected for the analysis.

$$P_{PV,t} = P_{r,PV} f_{PV} \left(\frac{\overline{G_{T,t}}}{\overline{G_{T,STC}}} \right), \forall t \in T \quad (2.10)$$

Since photovoltaic power is pollution free and it does not consume fossil fuel to generate electricity, we only consider capital cost and O&M cost. Capital cost (investment cost) is proportional to its installed capacity, and it can be seen as the fixed cost of microgrid operation. While O&M cost is related to the generation output at each hour, which should be obtained through optimization.

$$P_{r,PV} = P_{PV}^{cap} \quad (2.11)$$

$$C_{PV}^{cap} = P_{PV}^{cap} C_{PV,u}^{cap} \quad (2.12)$$

$$C_{PV,t}^m = C_{PV}^m P_{PV,t} \quad (2.13)$$

2.5 Wind Turbine (WT)

Wind power generation is one of the fastest-growing techniques and it is more easily to be large-scale connected to the power grids. WTs working on a simple principle: the wind turns the two or three blades around a rotor connected to the main shaft. The shaft spins and is connected to a generator that generates electric power.

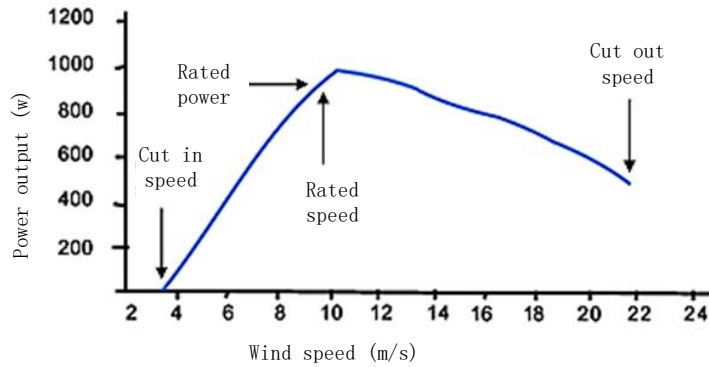


Figure 2-3. Power output of wind turbine under different wind speed

For WT, there are three important wind speed point: cut-in speed, cut-out speed as well as rated wind speed. Cut-in speed is the point at which the turbine starts producing electricity from turning. The cut-out point denotes how fast the turbine can go before

wind speeds get so fast that it risks damage from further operation. And if the ambient wind speed is equal to the rated wind speed, WT can operate at its optimal working point. Wind speeds both lower or higher than this value are probably to generate less power. Fig. 2-3 shows the relationship between WT output and ambient wind speed.

According to the principles of WT generation, the electric output power of WT can be expressed as:

$$P_{WT,t} = \begin{cases} 0, & 0 \leq v_t \leq v_{ci} \\ \lambda_1 v_t^2 + \lambda_2 v_t + \lambda_3, & v_{ci} \leq v_t \leq v_{co} \\ P_{r,WT}, & v_{rate} \leq v_t \leq v_{co} \\ 0, & v_{co} \leq v_t \end{cases}, \quad \forall t \in T \quad (2.14)$$

Like PV, WT is environmentally friendly and does not consume primary energy, thus only the capital cost and (O&M) cost are considered in the model, which can be formulated as:

$$C_{WT,t}^m = C_{WT}^m P_{WT,t} \quad (2.15)$$

$$P_{r,WT} = P_{WT}^{cap} \quad (2.16)$$

$$C_{WT}^{cap} = P_{WT}^{cap} C_{WT,u}^{cap} \quad (2.17)$$

2.6 Energy Storage (ES)

Nowadays, energy storage is a highly promising and frequently discussed topic in the energy community. Energy storage is a device that stores energy at a time and then uses it at a later time. In practice, it is usually utilized to buffer the fluctuations of solar power as well as the achievement of peak shaving. Besides, ES has the ability to decouple energy generation from consumption, resulting in lower operational costs.

Currently, there are many kinds of ES being used in MEMG, such as super-capacitor, flow battery, flywheel energy storage and compressed air energy storage. In terms of MEMG operation, we are more focusing on two kinds of ES: electrical energy storage (EES) and heat energy storage (HES).

To reflect the EES function, Li-ion battery is chosen as a reference for EES modeling for its widespread use in the power system.

The electric energy stored in ES at time t is related to the remaining energy at time $t-1$ as well as the charging/discharging power at that moment, which can be described as:

$$E_{EES,t} = (1 - \alpha)E_{EES,t-1} + [P_{EES,t}^{ch}\eta_{ch} - P_{EES,t}^{dis} / \eta_{dis}] \Delta t, \forall t \in T \quad (2.18)$$

Also, we should take its capital cost and O&M cost into consideration, which can be formulated as follows:

$$C_{EES}^{cap} = P_{EES}^{cap} C_{EES,u}^{cap} \quad (2.19)$$

$$C_{EES,t}^m = C_{EES}^m (U_{EES,t}^{ch} P_{EES,t}^{ch} + U_{EES,t}^{dis} P_{EES,t}^{dis}) \quad (2.20)$$

In a MEMG, peak heat load usually appears at 0-6 am when ambient temperature is low, while electricity is at its valley demand period because most of the consumers are sleeping at that time. In order to satisfy the thermal demands, the CHP plant needs to generate more thermal power, resulting in a large amount of electricity wasted. Utilizing HES is an efficient way to solve the mismatch between heat and electrical load, for the reason that HES can transfer the peak heat load to valley time periods, realizing the coordinated operation of thermal and electrical energy. Common HES mainly includes large heat storage tanks, regenerative electric boilers and so on [25, 26].

Note that Equation (2.18) is not always true at a time for both thermal and electrical storage units. In this regard, Ref. [27] presents a complete thermal storage tank model, which considers state transitions, power loss of HES. However, this thesis focuses on the

whole system and network-level coordinated dispatch of electricity and heat, therefore HST can be seen as similar to the EES [7]. The specific model of HST can be a promising future work in this research area. [7].

$$H_{HES,t} = (1 - \beta)H_{HES,t-1} + [P_{HES,t}^{ch}\lambda_{ch} - P_{HES,t}^{dis} / \lambda_{dis}]\Delta t, \forall t \in T \quad (2.21)$$

And the capital cost, O&M cost of HES can be modeled as:

$$C_{HES}^{cap} = P_{HES}^{cap} C_{HES,u}^{cap} \quad (2.22)$$

$$C_{HES,t}^m = C_{HES}^m (U_{HES,t}^{ch} P_{HES,t}^{ch} + U_{HES,t}^{dis} P_{HES,t}^{dis}) \quad (2.23)$$

2.7 Summary

With the development of energy internet, MEMG is an efficient way to integrate different kinds of DGs. Because there are many different units and components in electrical/heat network, and the operational characteristics of each unit are quite different, thus how to adequately model these units is the first step to do the optimal operation of MEMG.

Thus, this chapter first gives a short introduction to microgrid and MEMG, including their definition, structure as well as basic components. Next, the mathematical model of different units (including CHP plant, WT, PV, ES, EB) in MEMG are established, which mainly focuses on their external characteristics and economic items.

Chapter 3 District Heat Network (DHN)

3.1 Introduction

DHN continues to gain worldwide popularity for its benefits of increasing the efficiency of fuel use and flexibility of generation. Some studies have been done on the modeling of DHN. For instance, Reference [28] proposes a model for multi-district DHN based on the heat transfer theory. Also, the study in [14] considers thermal inertia of buildings and then presents an optimal operating model of DHN, which coordinates with the electrical network. Nevertheless, these research works assume that heat energy can be transferred to customers immediately, ignoring the transmission delay in DHN, which is not practical for industry engineering.

To fill this research gap, a more reasonable and systematic model of DHN is developed in this thesis. In this model, we consider the nodal flow balance constraints, mixing temperature equations and the quasi-dynamics of DHN. In order to model the transmission delay in DHN, a node method which is proposed in [12] is employed.

In this chapter, the introduction to the DHN, including its structure, working flow is given first. And then the mathematical equations of DHN are presented.

3.2 Introduction to DHN

A DHN is a system for providing thermal energy to residential, commercial and industrial customers. In DHN, heat is often produced by a heat source (like CHP plant, EB and so on) and then transferred through supply heat pipes to consumers. DHN transmission network consists of two parts: primary pipes as well as secondary pipes. Both two parts contain supply pipes and return pipes, which can be seen in Fig. 3-2.

Once heat is generated, it is directly transferred by high-temperature water through primary supply pipes. After entering the heat exchanger, hot water would be pumped into

the secondary network, and the temperature of the water would dramatically drop with the thermal energy delivered to consumers. Afterward, the cooled-down water would flow back through the return pipes to complete circulation. It should be noted that only the primary network is modeled since the length of the secondary pipes is much shorter than the primary pipes. Thus, it can be ignored without losing engineering accuracy [14].

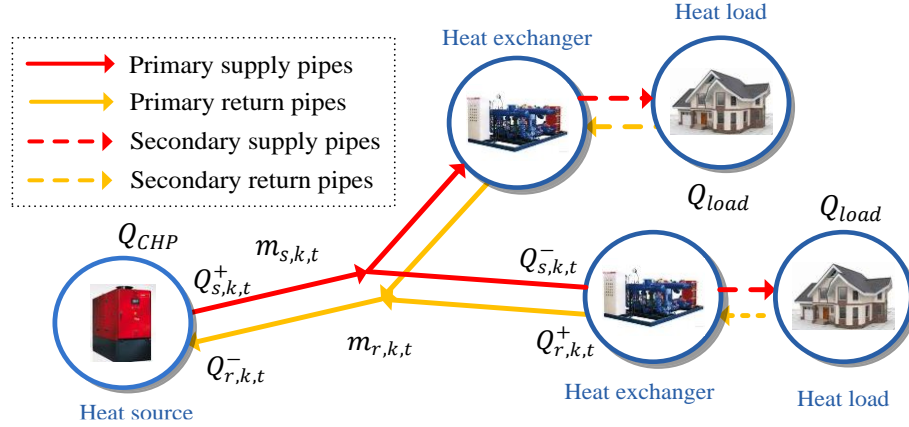


Figure 3-1. Schematic diagram of DHN.

Constant mass flow and variable temperature (CF-VT) control strategy has been widely conducted for the operation of DHN, especially in northern China [29]. Under this strategy, it is assumed that the mass flow rates in the network are constant whereas temperature is adjusted to meet the flexible thermal demands.

A DHN needs to satisfy some constraints, which are further discussed in the following part of this thesis.

3.3 DHN Modelling

3.3.1 Balance of Nodal Flow

In DHN, the mass rate of the water flowing into one node must be equal to that of the water mass flowing out. Eqs (3.1) and (3.2) denote the nodal mass balance constraints in the supply and return networks respectively.

$$\sum_{k \in K_{n,s}^-} m_{s,k,t} = \sum_{k \in K_{n,s}^+} m_{s,k,t}, \forall n \in N_{ps}, t \in T \quad (3.1)$$

$$\sum_{k \in K_{n,r}^-} m_{r,k,t} = \sum_{k \in K_{n,r}^+} m_{r,k,t}, \forall n \in N_{pr}, t \in T \quad (3.2)$$

3.3.2 Temperature Mixing

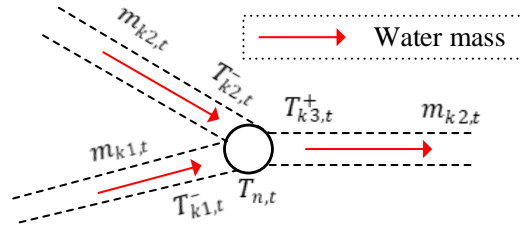


Figure 3-2. Water mass flowing in heat pipes.

As shown in the Fig.3-2, the temperature of every node is related to the temperature of previous water masses. According to the first law of thermodynamics, the temperature of the mixed water mass for each node can be calculated by Eqs. (3.3) and (3.4).

$$\sum_{k \in K_{n,s}^-} (T_{s,k,t}^- \cdot m_{s,k,t}) = T_{n,s}^m \sum_{k \in K_{n,s}^+} m_{s,k,t}, \forall n \in N_{ps}, t \in T \quad (3.3)$$

$$\sum_{k \in K_{n,r}^-} (T_{r,k,t}^- \cdot m_{r,k,t}) = T_{n,r}^m \sum_{k \in K_{n,r}^+} m_{r,k,t}, \forall n \in N_{pr}, t \in T \quad (3.4)$$

Besides, we assume that after the fusion of temperatures at node i , a mixing temperature filed is formed. The temperature of the mixed mass of node n is equal to the temperature at the starting point of all the pipes which are starting from node n .

$$T_{n,s}^m = T_{s,k,t}^+, \forall n \in N_{ps}, k \in K_{ns}^+, t \in T \quad (3.5)$$

$$T_{n,r}^m = T_{r,k,t}^+, \forall n \in N_{pr}, k \in K_{nr}^+, t \in T \quad (3.6)$$

3.3.3 Heat Power of Pipe

Based on the specific heat formula, the heat power should be equal to the multiplication of specific heat, temperature, and mass flow rate, which can be formulated as:

$$Q_{r,k,t}^+ = m_{r,k,t} \cdot C \cdot T_{r,k,t}^+ \cdot \alpha, \forall k \in K_{pr}, t \in T \quad (3.7)$$

$$Q_{r,k,t}^- = m_{r,k,t} \cdot C \cdot T_{r,k,t}^- \cdot \alpha, \forall k \in K_{pr}, t \in T \quad (3.8)$$

$$Q_{s,k,t}^+ = m_{s,k,t} \cdot C \cdot T_{s,k,t}^+ \cdot \alpha, \forall k \in K_{ps}, t \in T \quad (3.9)$$

$$Q_{s,k,t}^- = m_{s,k,t} \cdot C \cdot T_{s,k,t}^- \cdot \alpha, \forall k \in K_{ps}, t \in T \quad (3.10)$$

The relationship between the mass flow, inlet temperature, and heat energy is expressed in Eqs. (3.7)-(3.8). Because delivering hot water over a long distance brings about transmission delay and thermal loss, the temperature and heat energy at the ending point in a pipe is a little bit lower than that at the starting point. For this reason, two variables for temperature $T_{k,t}^+/T_{k,t}^-$ and heat power $Q_{k,t}^+/Q_{k,t}^-$ at the starting/ending point in a pipe are set in this model.

3.3.4 Temperature Quasi-Dynamics

Because the water flow rate is not as fast as the transmission speed of the electricity, there is usually a time delay ranging from minutes to hours during the heat transferring process. Thus, it is a practical need to consider the dynamic characteristics of pipes in heat network modeling. In this light, the node method which is proposed in [12, 30] is employed in this study. Fig. 3-3 illustrates the dynamic process of water flowing through a pipe. The temperature would drop slowly when water flows from starting point to ending point in a pipe, and the process is expressed in (3.11)-(3.26).

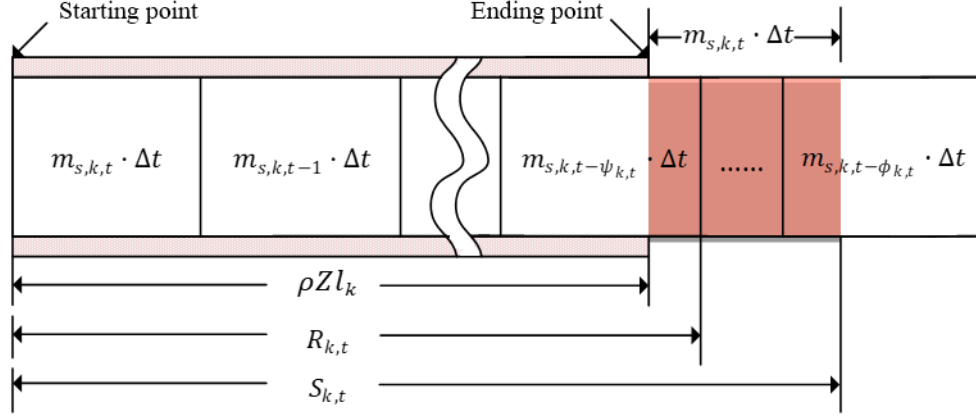


Figure 3-3. Vertical section of a heat pipe.

Firstly, the temperature at the ending point of the pipe without heat loss can be evaluated using the historic temperature at the starting point. Besides, the total transmission delay is related to the mass flow, which can be expressed as follows:

$$T_{s,k,t}^{-'} = \sum_{\omega=t-\phi_{k,t}}^{t-\psi_{k,t}} K_{k,t,\omega} T_{s,k,t}^{+}, \forall k \in K_{ps}, t \in T \quad (3.11)$$

$$T_{r,k,t}^{-'} = \sum_{\omega=t-\phi_{k,t}}^{t-\psi_{k,t}} K_{k,t,\omega} T_{r,k,t}^{+}, \forall k \in K_{pr}, t \in T \quad (3.12)$$

The vertical section of a heat pipe is shown in Fig. 3-3. The total volume of hot water in the pipe is assumed to be $\rho A l$ if the length of this pipe is l . cells in the horizontal direction represent a sequence of water masses in the pipeline. For instance, $m_{s,k,t} \cdot \Delta t$ stands for the water mass flows into the pipe at time t . The right-hand side blocks that are outside the pipe denote the water masses that have flowed out from that pipe.

Eqs. (3.11) and (3.12) can be seen as the DHN state transition equations, which are of great importance to consider the DHN's heat storage potential. The basic idea of these two mathematical expressions is that the temperature at the ending point of the pipe $T_{s,k,t}^{-'}$ and $T_{r,k,t}^{-'}$ without heat loss can be estimated by the average temperature of water masses flowing out the pipe during time t (the shaded area in Fig. 3-3. Here, some variables are used to explain the whole process exactly. For example, it is assumed that after $\psi_{k,t}$ time periods, the water mass starts to flow out, whereas after $\phi_{k,t}$ time

periods, the water mass of that cell totally flows out of the pipeline. The two different variables $\phi_{k,t}$ and $\psi_{k,t}$ are mathematically defined as (3.13) and (3.14) respectively.

$$\psi_{k,t} = \min_{n \in N} \left\{ n : s.t. \sum_{\omega=t-n}^t (m_{s,k,\omega} \cdot \Delta t) \geq \rho A l_k \right\} \quad (3.13)$$

$$\phi_{k,t} = \min_{m \in N} \left\{ m : s.t. \sum_{\omega=t-m}^t (m_{s,k,\omega} \cdot \Delta t) \geq \rho A l_k + (m_{s,k,t} \cdot \Delta t) \right\} \quad (3.14)$$

The symbol $R_{k,t}$ represents the total hot water volume flowing into the pipe k from period $t - \psi_{k,t}$ to period t . Similarly, $S_{k,t}$ denotes the total hot water volume flowing into the pipe k from period $t - \phi_{k,t}$ to period t , just as shown in Fig. 3-3.

$$R_{k,t} = \sum_{k=t-\psi_{k,t}}^t (m_{s,k,t} \cdot \Delta t) \quad (3.15)$$

$$S_{k,t} = \begin{cases} \sum_{k=t-\phi_{k,t}+1}^t (m_{s,k,t} \cdot \Delta t), & \text{if } \phi_{k,t} \geq \psi_{k,t} + 1 \\ R_{k,t}, & \text{otherwise} \end{cases} \quad (3.16)$$

Based on this, the temperature $T_{k,t}^{-}$ at the ending point of each pipe without considering the heat loss can be calculated by Eqs. (3.17).

$$T_t^{-} = \frac{1}{m_t \cdot \Delta t} \left[(R_t - \rho A l) \cdot T_{t-\psi_t}^{+} + \sum_{\omega=t-\phi_t+1}^{t-\psi_t-1} (m_{\omega} \cdot \Delta t \cdot T_{\omega}^{+}) + (m_{\omega} \cdot \Delta t + \rho A l - S_t) \cdot T_{t-\phi_t}^{+} \right] \quad (3.17)$$

Compared Eqs. (2.11), (2.12) and (2.17), we can get that the variable $K_{k,t,\omega}$ can be defined as:

$$K_{k,t,\omega} = \begin{cases} (m_{s,k,t} \cdot \Delta t - S_{k,t} + \rho Z L_k) / (m_{s,k,t} \cdot \Delta t), & \omega = t - \phi_{k,t} \\ (m_{s,k,\omega} \cdot \Delta t) / (m_{s,k,t} \cdot \Delta t), & \omega = t - \phi_{k,t} + 1, \dots, t - \psi_{k,t} - 1 \\ (R_{k,t} - \rho Z L_k) / (m_{s,k,t} \cdot \Delta t), & \omega = t - \psi_{k,t} \\ 0, & \text{otherwise} \end{cases} \quad (3.18)$$

The coefficients $\phi_{k,t}$, $\psi_{k,t}$ and $K_{k,t,\omega}$ are constants under the CF-VT (constant mass flow and variables temperature) control strategy. However, under the VF-VT (variable

mass flow and variable temperature) control strategy, they will vary with the water mass flow.

Secondly, to take the heat loss into consideration, the temperature drop caused by heat loss can be calculated and used to modify the actual temperature at the ending point of pipes.

$$T_{s,k,t}^+ = T_{am,t} + J_{k,t} \left(\sum_{\omega=t-\phi_{k,t}}^{t-\psi_{k,t}} K_{k,t,\omega} T_{s,k,\omega}^+ - T_{am,t} \right) \quad (3.19)$$

$$T_{r,k,t}^- = T_{am,t} + J_{k,t} \left(\sum_{\omega=t-\phi_{k,t}}^{t-\psi_{k,t}} K_{k,t,\omega} T_{r,k,\omega}^- - T_{am,t} \right) \quad (3.20)$$

These two equations consider the temperature loss during the heat transferring process due to the ambient heat loss. Besides, the variable $J_{k,t}$ in Eqs. (2.17) and (2.18) can be defined as:

$$J_{k,t} = \exp \left[-\frac{\lambda \Delta t}{A \rho C} \right] \left(\psi_{k,t} + \frac{1}{2} + \frac{S_{k,t} - R_{k,t}}{m_{s,k,t-\psi_{k,t}} \Delta t} \right) \quad (3.21)$$

3.3.5 Heat loads

Heating buildings for dwellers is the major heat load in winter, normally taking up 80%-90% of the total heat loads (not including heating processes of industry) and having a huge potential for regulation. Thus, this thesis focuses on the modeling of buildings. Heat loads are the quantity of heating energy that must be used to warm buildings so as to keep people comfortable. Eq. (3.26) indicates that the amount of required heat loads is related to the planar area of buildings and the ambient outside temperature at that moment [14]. The heat energy would be transferred through the primary heat exchanger and radiator before it enters buildings. Eqs. (3.22) to (3.26) describe the transferring process.

$$Q_{s,k,t}^+ - Q_{r,k,t}^- = (P_{CHP} \cdot \eta_{heat} + Q_{eb} \cdot \eta_{eb}) \cdot \eta_{hex1}, k \in K_{hs}, t \in T \quad (3.22)$$

$$m_{s,k,t} = m_{r,k,t}, \forall k \in K_{hs}, t \in T \quad (3.23)$$

$$Q_{s,k,t}^- - Q_{s,k,t}^+ = H_{load,j} / \eta_{ra}, k \in K_{hl}, t \in T \quad (3.24)$$

$$m_{s,k,t} = m_{r,k,t}, \forall k \in K_{hl}, t \in T \quad (3.25)$$

$$H_{load,l,t} = G_l A_l (T_{design} - T_{am,t}), \forall l \in L, t \in T \quad (3.26)$$

3.4 Summary

In this chapter, the basic structure and working flow of DHN have been introduced firstly. Following that, the main content of this chapter is the modeling of DHN, including the nodal flow balance constraints, mixing temperature equations, quasi-dynamics, and transmission delay. The content of Chapter 3 is of great significance to Chapter 4 and lays a solid foundation for the following contents. It is worth to mention that the detailed data and variables indexes for the same unit in Chapters 4, 5 and 6 may be different from this chapter.

Chapter 4 Optimally Coordinated Operation of a MEMG with Coupled Heat and Electrical Networks

4.1 Introduction

Satisfying different kinds of energy demands such as heating, cooling as well as electricity of local industrial/commercial/residential customers is essential for improving the urban environment and achieving certain social and economic benefits. MEMGs integrating DGs like PVs, WTs, CHP plants can simultaneously provide a comprehensive energy supply. There are several kinds of energy balance flows in a MEMG, like heating energy flow, cooling energy flow, electrical energy flow, etc. How to optimally dispatch the working units and loads in MEMG based on the specific properties of different energy flows has been highly regarded today. In the meantime, energy utilization efficiency and environmental benefits are two main evaluating indicators for CHP systems, which can be employed to decide the operation mode of some components in MEMG.

In traditional coupled heat and electrical network, considering the internal characteristics of microturbine, the CHP system usually works in FHL (following heat load) mode. Under FHL mode, the power output of the CHP plant satisfies heat requirements at first. According to Eqs. (2.1) and (2.2), the power output of CHP plant is proportional to its heat power output, thus, the electric power of CHP would be determined according to its heat power (if the maximum heat output could not meet the thermal demands, MEMG would seek help from HES or EB) [31, 32]. Meanwhile, RES generation enjoys the advantages of pollution-free and less energy consumption, thus in MEMG's operation, renewable generators work at maximum power point tracking mode for reducing curtailment of wind/solar power. In this chapter, how to optimally dispatch all the DGs and ancillary units in MEMG based on their own characteristics and system operational constraints.

In this chapter, an optimal operation method of MEMG with coupled heat and power networks is proposed, aiming to minimize the system operational costs while satisfying all the technical constraints. The proposed approach is converted to a mix-integer linear programming (MILP) problem for fast solution speed. Next, several cases are simulated to show the advantages of the proposed method and the benefits of considering the transmission delay in DHN. Simulation results verify that combining both heat network and electric network introduces more dispatch flexibility and economic benefits of MEMG.

4.2 Model of the Proposed Method

4.2.1 Objective Function

The structure of a CCHP-based MEMG in this chapter is the same as Fig.1-2. Because renewable generators like PV and WT don't consume fossil fuels to generate electricity, their generation costs (fuel costs) are negligible compared to the CHP plant. What's more, when the microgrid is working on grid-connected mode, the power mismatch can be compensated by the utility grid (i.e., purchase electricity from the main grid to satisfy the consumers' requirements and sell electricity so as to improve economic returns), thus, no power surplus or shortage will suddenly appear. In the MEMG operation, the goal is to reduce the daily operation cost C_{total} while satisfying all the constraints of the components and the whole system. The total cost contains the capital cost of each component C_{cp} , fuel cost $C_{f,t}$, operation & maintenance (O&M) cost $C_{om,t}$, the average daily cost of laying pipes C_n as well as the revenue of selling heat to customers $C_{s,t}$.

Besides, it should be noted that since we integrate the specific model of DHN (including its transmission delay) in this method, DHN can be utilized as a HES to release/store heat energy (which would be further discussed in the following contents), thus we only employ EES in this chapter.

$$MINC_{total} = C_{CP} + C_n + \sum_{t=1}^T (C_{f,t} + C_{e,t} + C_{om,t} - C_{s,t}) \Delta t \quad (4.1)$$

$$C_{CP} = \sum_{u=1}^U (C_{CP}^u \cdot C_{ap}^u) \cdot \left[\frac{I(1+I)^{Y^u}}{(1+I)^{Y^u} - 1} \right] \quad (4.2)$$

$$C_{f,t} = [C_{CH4} \cdot (P_{CHP,t} / \eta_{CHP})] / L_{HVNG} \quad (4.3)$$

$$C_{e,t} = C_{gd,t} \cdot P_{gd,t} - C_{sd,t} \cdot P_{sd,t} \quad (4.4)$$

$$C_n = C_{pipe} \cdot \left(\sum_{k \in K_{ps} + K_{ps}} l_k \right) \quad (4.5)$$

$$C_{om,t} = C_{EB}^{om} \cdot \left(\sum_{i \in I} P_{EB,t}^i \right) \Delta t + C_{MT}^{om} \cdot \left(\sum_{i \in I} P_{CHP,t}^i \right) \Delta t + C_{WT}^{om} \cdot \left(\sum_{i \in I} P_{WT,t}^i \right) \Delta t \\ + C_{PV}^{om} \cdot \left(\sum_{i \in I} P_{PV,t}^i \right) \Delta t + C_{EB}^{om} \cdot \sum_{i \in I} (P_{ESC,t}^i + P_{ESD,t}^i) \Delta t \quad (4.6)$$

$$C_{s,t} = C_H \cdot \sum_{l \in L} H_{load,l,t} \quad (4.7)$$

Also, it is worth to mention that Eq (4.1) calculates the equivalent annual cost (EAC) of each component in MEMG, which considers the annual interest rate.

4.2.2 Constraints

The generation output of DGs (WT, PV, CHP) and ancillary device (EB) should be within their technical limits, and the incremental change of the units within a short time period is limited by its ramping capability. These constraints can be expressed as:

$$P_{CHP}^{MIN} \leq P_{CHP,t}^i \leq P_{CHP}^{MAX} \quad (4.8)$$

$$-R_{CHP}^{down} \Delta t \leq P_{CHP,t}^i - P_{CHP,t-1}^i \leq R_{CHP}^{up} \Delta t \quad (4.9)$$

$$P_{WT}^{MIN} \leq P_{WT,t}^i \leq P_{WT}^{MAX} \quad (4.10)$$

$$-R_{WT}^{down} \Delta t \leq P_{WT,t}^i - P_{WT,t-1}^i \leq R_{WT}^{up} \Delta t \quad (4.11)$$

$$P_{PV}^{MIN} \leq P_{PV,t}^i \leq P_{PV}^{MAX} \quad (4.12)$$

$$-R_{PV}^{down} \Delta t \leq P_{PV,t}^i - P_{PV,t-1}^i \leq R_{PV}^{up} \Delta t \quad (4.13)$$

$$P_{EB}^{MIN} \leq P_{EB,t}^i \leq P_{EB}^{MAX} \quad (4.14)$$

$$-R_{EB}^{down} \Delta t \leq P_{EB,t}^i - P_{EB,t-1}^i \leq R_{EB}^{up} \Delta t \quad (4.15)$$

As for EES, state limit, charging/discharging power constraints, energy limit should be satisfied, which are presented in Eqs. (4.16)-(4.20).

$$0 \leq P_{EES,t}^{dis,i} \leq U_{EES,t}^{dis,i} \cdot P_{ESD}^{MAX} \quad (4.16)$$

$$0 \leq P_{EES,t}^{ch,i} \leq U_{EES,t}^{ch,i} \cdot P_{ESC}^{MAX} \quad 0 \leq P_{EES,t}^{ch,i} \leq U_{EES,t}^{ch,i} \cdot P_{ESC}^{MAX} \quad (4.17)$$

$$\mu_{EES}^{MIN} \cdot E_{EES}^{cap} \leq E_{EES,t}^i \leq \mu_{EES}^{MAX} \cdot E_{EES}^{cap} \quad (4.18)$$

$$U_{EES,t}^{ch,i} + U_{EES,t}^{dis,i} \leq 1 \quad (4.19)$$

$$E_{EES,0}^i = E_{EES,N\Delta t}^i \quad (4.20)$$

Equation (4.20) denotes that the electric energy stored in EES at the beginning of the day should be equal to the energy stored at the end of the day.

Besides, we assume that the MEMG is based on the radical distribution network in this thesis, accordingly, it must first satisfy the distribution network power flow constraints [33], which can be presented in (4.21) to (4.27).

$$P_{i+1,t} = P_{i,t} + P_{G,i,t} - P_{load,i,t} \quad (4.21)$$

$$Q_{i+1,t} = Q_{i,t} + Q_{G,i,t} - Q_{load,i,t} \quad (4.22)$$

$$V_{i+1,t} = V_{i,t} - \frac{r_i P_{i,t} + x_i Q_{i,t}}{V_0} \quad (4.23)$$

$$1 - \Delta V_{\max} \leq V_{i,t} \leq 1 + \Delta V_{\max} \quad (4.24)$$

$$P_{G,i,t} = \sum_{i \in I} P_{MT,t}^i + \sum_{i \in I} P_{WT,t}^i + \sum_{i \in I} P_{PV,t}^i + \sum_{i \in I} (P_{EES,t}^{dis,i} + P_{EES,t}^{ch,i}) - \sum_{i \in I} P_{EB,t}^i \quad (4.25)$$

$$-P_{\max} \leq P_{i,t} \leq P_{\max} \quad (4.26)$$

$$-Q_{\max} \leq Q_{i,t} \leq Q_{\max} \quad (4.27)$$

To protect the thermal pipes in DHN, their inside temperature should be in a range.

$$T_s^{\min} \leq T_{s,k,t}^+ \leq T_s^{\max}, \forall k \in K_{ps}, t \in T \quad (4.28)$$

$$T_s^{\min} \leq T_{s,k,t}^- \leq T_s^{\max}, \forall k \in K_{ps}, t \in T \quad (4.29)$$

$$T_r^{\min} \leq T_{r,k,t}^+ \leq T_r^{\max}, \forall k \in K_{pr}, t \in T \quad (4.30)$$

$$T_r^{\min} \leq T_{r,k,t}^- \leq T_r^{\max}, \forall k \in K_{pr}, t \in T \quad (4.31)$$

Other constraints of heat networks are listed in the last chapter (3.1)-(3.26).

4.2.3 Solution Algorithm

Because the mass flow rates of hot water are constants under the CF-VT control strategy, the objective and constraints which are listed before form a MILP problem, so that it can be handled directly by some existing commercial solvers. The whole problem is formulated as follows [34]:

$$\min f(x, y) \quad (4.32)$$

$$s.t. \begin{cases} h_k(x, y) = 0, k = 1, 2, \dots, m \\ g_l(x, y) \leq 0, l = 1, 2, \dots, n \\ x_{\min} \leq x \leq x_{\max} \\ y \in \{0, 1\} \end{cases} \quad (4.33)$$

where the decision variable x stands for the power outputs/inputs of controllable units, charging/discharging power of EES in the MEMG as well as the power exchanged with the utility grid. Variable y denotes the on/off status of the CHP plant and EB, charge/discharge state of EES, and the exchanging power state with the utility grid. Besides, equality constraints $h_k(x, y)$ include the reactive/active power flow balance at each bus, the nodal mass flow balance at each node in DHN and so on, while inequality

constraints $g_l(x, y)$ contain operational constraints of all the units, the maximum/minimum temperature limits of thermal pipes, etc.

4.3 Case Studies

4.3.1 Tested System

Fig.4-1 presents the schematic diagram of the tested system, which is based on the IEEE 33-bus radial distribution network [35]. Besides, a 13-pipe DHN is also integrated into the MEMG, as shown in Fig. 4-1 (red lines). In the tested MEMG, V_0 is set to be 1.0 p.u. and ΔV_{\max} is $\pm 5\%$ of the nominal level [36]. In fig. 4-1, “K” denotes “pipe” whereas “L” denotes “heat load”. There are three heat sources (CHP plants) in this MEMG, located at bus 6, 17 and 32 respectively. Table. 4-1 shows the location of each unit.

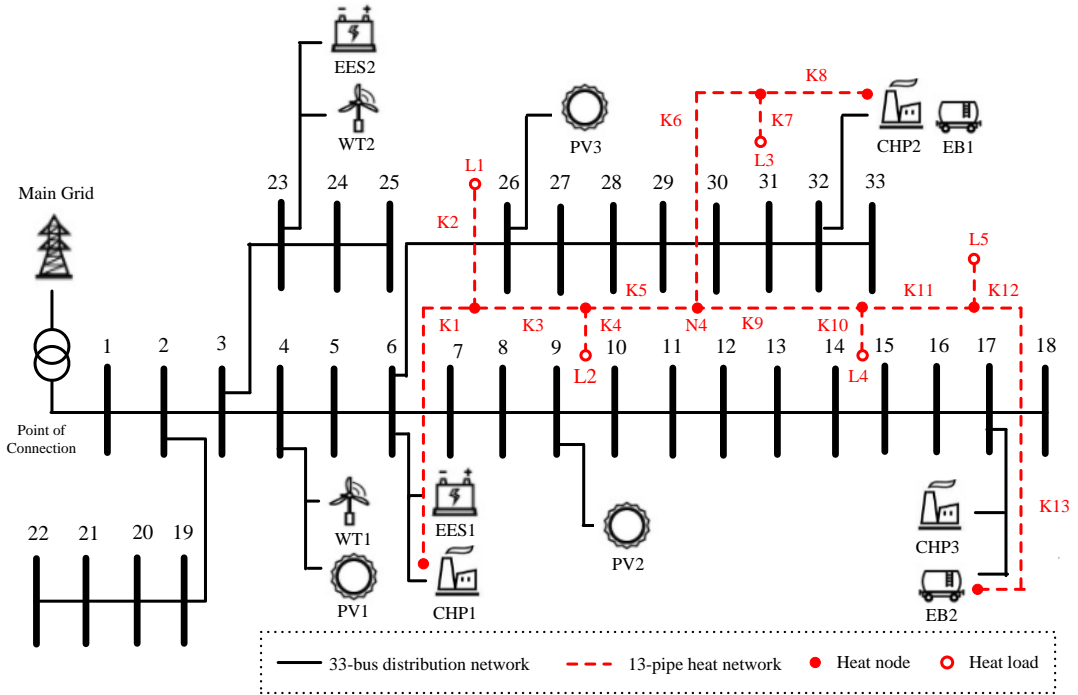


Figure 4-1. Schematic diagram of the tested MEMG.

In order to get more practical simulation results, we collected the weather condition data from a winter day in Beijing, China. The predicted PV, WT electric outputs and the ambient temperature over 24 hours are shown in Fig. 4-2. The electricity price for the whole day can be seen in Fig. 4-3. Apart from that, Table. 4-2 shows the parameters of

different working units in the tested MEMG. The parameters of heat pipes and DHN are presented in Table 4-3 and 4-4 respectively. Table 4-5 gives the parameters of EES. Apart from that, the mass flow rate of each pipe is listed in Table 4-6 and the impedance of each bus is presented in Table 4-7.

Table 4-1. System parameters

Component	Location in EN	Location in DHN
PV	Bus4, Bus9, Bus26	/
WT	Bus4, Bus23	/
EES	Bus6, Bus23	/
CHP	Bus6, Bus32, Bus17	Node1, Node6, Node9

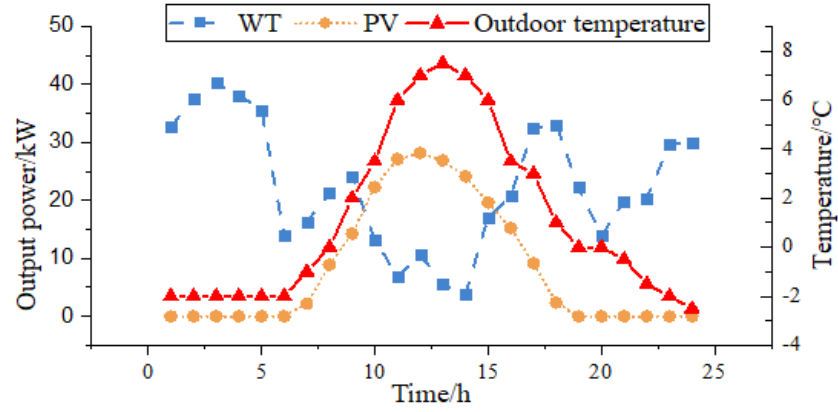


Figure 4-2. Predicted weather condition data over 24 hours.

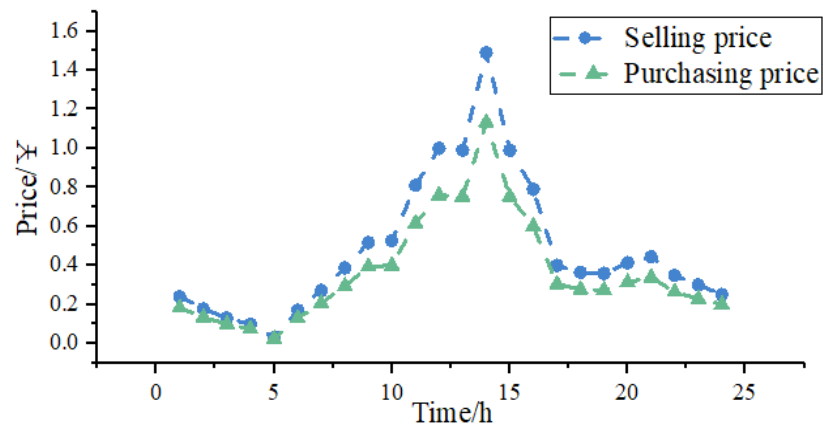


Figure 4-3. Electricity price for the whole day.

Table 4-2. Parameters of working units in MEMG

Type	C_{cp}	C_{om}	P^{max}	P^{min}	R^{down}	R^{up}	Y^u
------	----------	----------	-----------	-----------	------------	----------	-------

<i>CHP</i>	10000	0.1250	300	60	5	10	25
<i>PV</i>	2000	0.0133	30	0	/	/	25
<i>WT</i>	5000	0.0145	55	0	/	/	20
<i>EB</i>	1000	0.0089	150	0	2	3	15

Table 4-3. Heat pipe parameters

Pipe	Length	Pipe	Length	Pipe	Length
K1	700	K6	500	K10	400
K2	400	K7	400	K11	500
K3	400	K8	500	K12	400
K4	500	K9	500	K13	400
K5	400				

Table 4-4. DHN parameters

Name	Value	Name	Value	Name	Value
ρ	1	R	0.0002	η_{hex1}	0.9
η_{ra}	0.9	I	0.05	C_H	0.1

Table 4-5. Parameters of EES [7]

Name	Value	Name	Value	Name	Value
μ_{ES}^{MIN}	0.15	μ_{ES}^{MAX}	0.85	C_{ES}^{om}	0.073
C_{cp}^{ES}	670	$\eta_{ESC/ESD}$	0.9	α_{ES}	0.001
P_{ESC}^{MAX}	50	P_{ESD}^{MAX}	50	E_{ES}^{cap}	180

Table 4-6. Mass flow rate of each pipe

Pipe	Mass flow	Pipe	Mass flow	Pipe	Mass flow
K1	2400	K6	1600	K10	800
K2	800	K7	2400	K11	1600
K3	1600	K8	800	K12	800
K4	800	K9	800	K13	2400
K5	800				

Table 4-7. Impedance of each bus [37]

Bus	R_i	X_i	Bus	R_i	X_i
1→2	0.0922	0.0470	17→18	0.7320	0.5740
2→3	0.4930	0.2511	2→19	0.1640	0.1565
3→4	0.3660	0.1864	19→20	0.5042	1.3554
4→5	0.3811	0.1941	20→21	0.4095	0.4784

5→6	0.8190	0.7070	21→22	0.7089	0.9373
6→7	0.1872	0.6188	3→23	0.4512	0.3083
7→8	0.7114	0.2351	23→24	0.8980	0.7091
8→9	1.0300	0.7400	24→25	0.8960	0.7011
9→10	1.0440	0.7400	6→26	0.2030	0.1034
10→11	0.1966	0.0650	26→27	0.2842	0.1447
11→12	0.3744	0.1238	27→28	1.0590	0.9337
12→13	1.4680	1.1550	28→29	0.8042	0.7006
13→14	0.5416	0.7129	29→30	0.5075	0.2585
14→15	0.5910	0.5260	30→31	0.9744	0.9630
15→16	0.7463	0.5450	31→32	0.3105	0.3619
16→17	1.2890	1.721	32→23	0.3410	0.5302

In order to show the validity of the proposed approach in this chapter, three cases are conducted.

Case1: In this case, it is assumed that there is no topology and specific model of heat network, thus $C_n=0$. That is to say, only the constraints of the electrical network (2.1) to (2.20) and (4.1) to (4.27) are considered. Besides, each heat load (building) is supplied by nearby CHP plants or EBs.

Case2: In this case, we assume that heat energy can be transferred to the customers immediately without any time delay, just like the electrical network. In other words, DHN is static without dynamic characteristics. In addition to the electrical network constraints, DHN constraints (3.1) to (3.10), (3.22) to (3.26) and (4.28) to (4.31) are also taken into consideration. Apart from that, using Eqs. (3-34)-(3-37) to calculate heat loss during the transferring process and then replace Eqs. (3.11)-(3.21).

$$Q_{s,k,t}^- = (1 - \mu_{k,t} \cdot l_k) \cdot Q_{s,k,t}^+, \forall k \in K_{ps}, t \in T \quad (4.34)$$

$$Q_{r,k,t}^- = (1 - \mu_{k,t} \cdot l_k) \cdot Q_{r,k,t}^+, \forall k \in K_{pr}, t \in T \quad (4.35)$$

$$\mu_{k,t} = (2\pi / R) \cdot (T_{k,t}^{avg} - T_{am,t}), \forall k \in K, t \in T \quad (4.36)$$

$$T_{k,t}^{avg} = T_{k,t}^- e^{-\frac{2\pi}{\rho CR} l_k} + (1 - e^{-\frac{2\pi}{\rho CR} l_k}) T_{am,t}, \forall k \in K, t \in T \quad (4.37)$$

Case3: In this case, the proposed system-wide coordinated method is employed, in which the electrical and heat network are highly coupled.

The detailed constraints which are taken into consideration in the three cases are summarized in Table. 4-8.

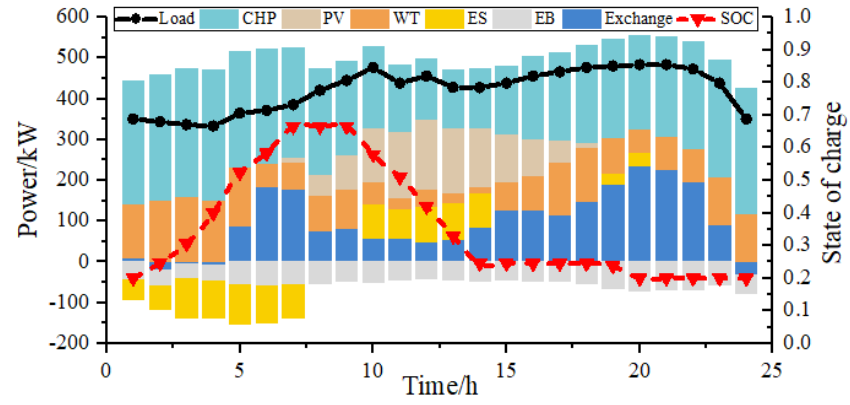
It should be noted that other practical parameters can also be employed to the proposed method, which would not significantly influence its effectiveness. The case studies are conducted on an Intel(R) Core i5-7200U, 2.50-GHz personal computer with 8GB of memory. The optimization problem is solved by a commercial software called General Algebraic Modelling System (GAMS). Besides, the unit dispatching time is set to be 1 hour.

Table 4-8. Cases summary

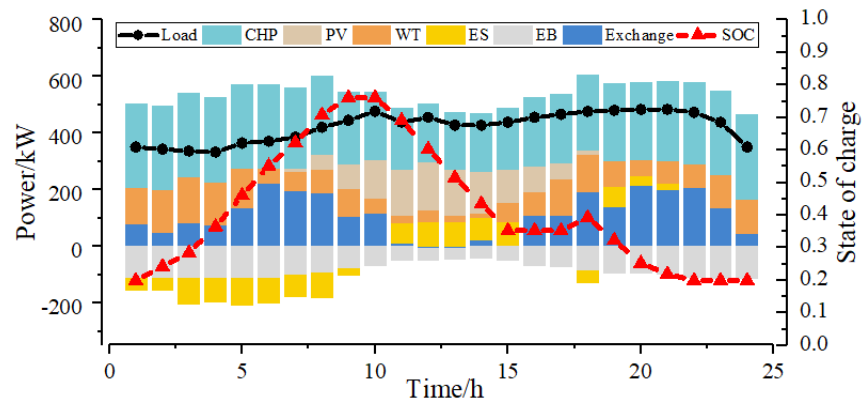
<i>Cases</i>	Power network constraints	Static DHN constraints	Dynamic characteristics of DHN
<i>Case1</i>	√		
<i>Case2</i>	√	√	
<i>Case3</i>	√	√	√

4.3.2 Simulation Results

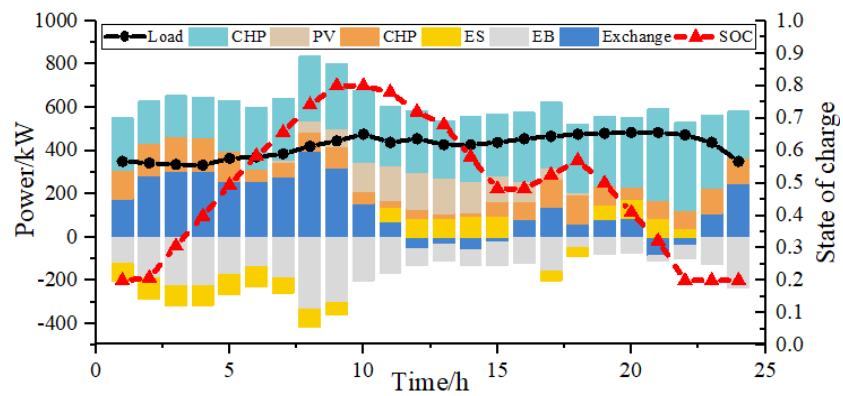
The simulation results of power balance conditions in case1, 2, 3 can be found in Fig. 4-4 (a),(b),(c) respectively. SOC stands for the state of charge of EES, which cannot be measured directly but can be estimated from direct measurement variables. It can be seen from Fig. 4-4 the electrical loads can be fully satisfied under these three cases. From 7 AM to 6 PM, PV generates electricity because of the sufficient solar irradiation. EB consumes excess electricity to produce thermal energy, in order to reduce the waste energy caused by the mismatch between heat and electricity. Fig. 4-4 demonstrates that all the working units in MEMG can be optimally scheduled according to their external characteristics and technical constraint. In order words, the proposed system-wide coordinated operation method is effective in optimally scheduling all the components to satisfy the diversity (heat and electricity) load demands.



(a)



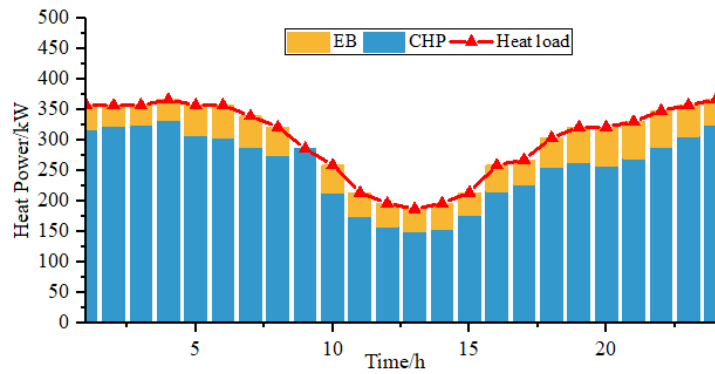
(b)



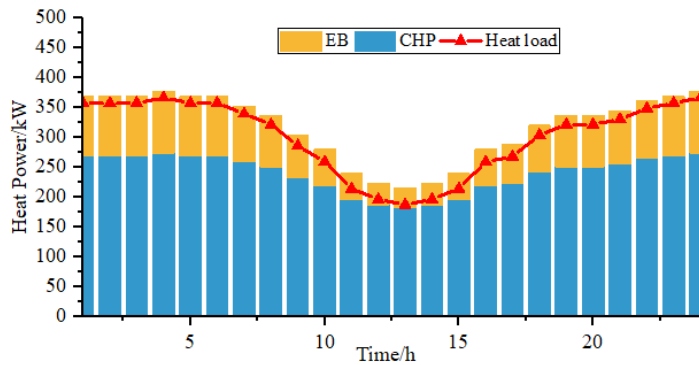
(c)

Figure 4-4. Power balance conditions. Case1 (a), Case2 (b), Case3 (c).

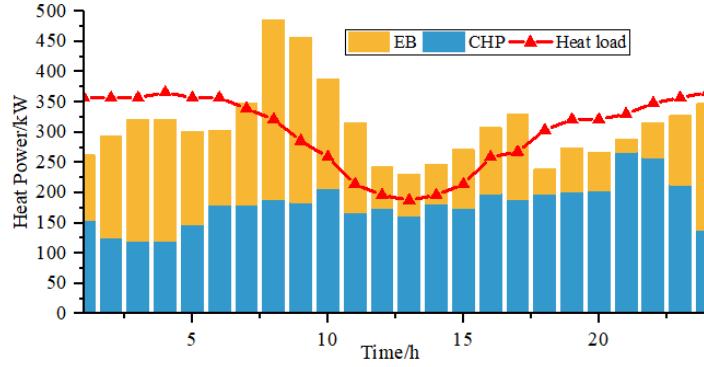
The heat balance conditions under three cases are shown in Fig. 4-5. In Case1, heat energy is almost all generated by CHP units. The main reason is that in case1, no specific model of DHN is considered, long-distance heat energy transmission cannot be achieved, thus only the nearest CHP plant can provide heat energy to consumers, resulting in more generation from CHP plants in Case1. Because the unit generation cost and operation cost of CHPs are much higher than that of EBs (which can be found in Table 4-2), the total cost of Case1 is the highest (9122.83¥) among all the three cases. While in the latter two cases, the specific model of DHN is taken into consideration, the limits of transferring distance can be broken, hence more EBs are committed in these two cases. Consequently, Case2 and Case3 cost less than Case1 (8450.01¥ and 7960.72¥ respectively).



(a)



(b)



(c)

Figure 4-5. Heat conditions. Case1 (a), Case2 (b), Case3 (c).

Fig.4-5 and Fig. 4-6 shows the total heat output (including the heat generation of EBs and CHPs) under three cases. It can be observed that in Case1, the total heat generation is exactly equal to the heat loads at each hour. In Case2, the specific static model of DHN is considered, and total heat generation is a little bit larger than the heat loads, accounting for the effect of temperature loss of the fluid. It is noted in Case3 that the total heat generation does not always match the heat loads at each hour. This is mainly because when the transmission delay in heat pipes is modeled, heat generation and consumption can appear at different periods during a day. Hence, DHN can be utilized as a heat storage tank storage (HST) from the system's point of view. For instance, from 1 am to 5 am, the design thermal load is at its peak owing to the cold weather outside, but the power loads are low because many consumers are still sleeping. In traditional following heat load (FHL) mode or in Case 1, CHPs need to generate more power to satisfy the high heat loads, resulting in some energy waste. Nevertheless, in Case3, during that time, the internal temperature in heat pipes would drop, and this part of the energy will be supplied to the customers, which acts like an HST releases heat energy. As a result, the heat power of CHP units can be dramatically reduced. In other words, CHPs and EBs supplies the heat energy in priority, and DHN acts as a supplement in the proposed method.

However, the internal temperature of heat pipes should be controlled within a range (usually supply pipes: 75°C-95°C; return pipes 55°C-75°C), thus DHN's storage capacity is limited compared to conventional HST.

Simulation results demonstrate that in the proposed method, DHN and electrical network are highly coupled, and DHN can be seen as an HST with limited capacity when its quasi-

dynamic characteristics and time delay are considered. The storage status of DHN for the whole day is demonstrated in Fig. 4-7.

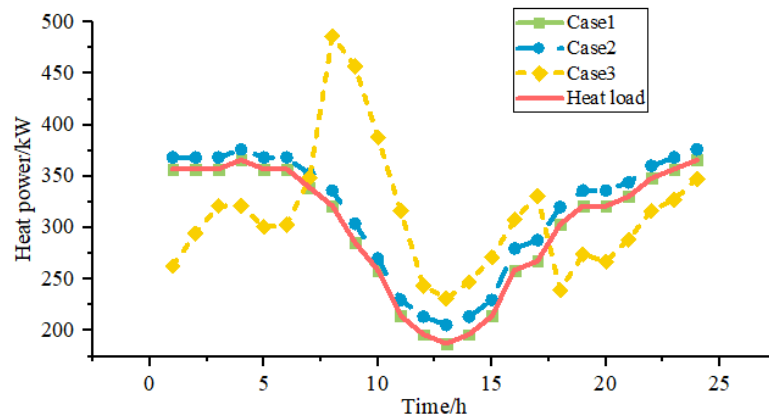


Figure 4-6. Heat generated by CHP and EB in the three cases.

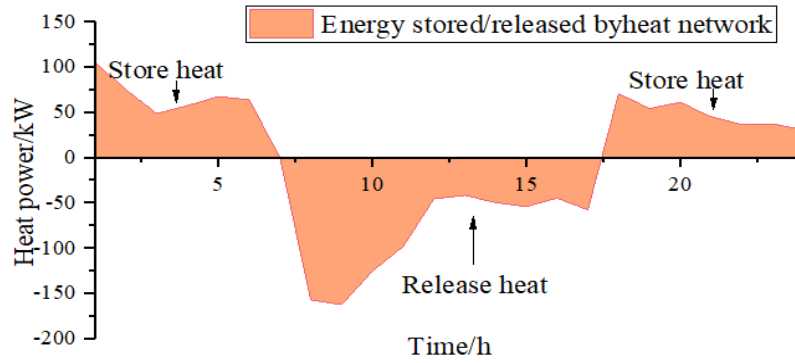


Figure 4-7. Storage status of heat network of 24 hours under Case3.

Table 4-9. Simulation results

<i>Cost/revenue item</i>	Case 1	Case 2	Case 3
<i>Capital cost</i>	4840.76	3015.74	3015.74
<i>Cost of laying heat pipelines</i>	0	1958.90	1958.90
<i>Fuel cost</i>	3008.62	2366.04	2102.98
<i>O&M cost</i>	1375.01	1126.70	1061.56
<i>Power exchange cost</i>	670.07	754.26	593.17
<i>Heat revenue</i>	771.63	771.63	771.63
<i>Total cost</i>	9122.83	8450.01	7960.72

The total costs under three cases are summarized in Table 4-9. As discussed before, in case1, heat energy cannot be transferred through long distances. Hence, five CHPs are placed nearby to meet thermal demands, which leads to the highest capital cost

(¥4840.76). While in Case2 and Case3, this kind of limitation is broken because of DHN. Although we need to pay more on laying DHN, the system cost is 7% lower than that of Case1. In other words, considering the specific model of DHN introduces more overall economic benefits. In Case3, the total cost is ¥1162.11 less than that of Case1, giving a saving rate of 12.7%. Simulation results show that the proposed method encourages a higher energy utilization rate and cut down the operating cost in MEMG.

4.4 Summary

This chapter presents an optimal coordinated operation method for MEMGs. The objective of this method is to minimize the total system cost, including capital cost, O&M cost, fuel cost and so on. In the proposed method, both the constraints of DHN and electrical network are systematically modeled, thus DHN and electric power grids strongly interact with each other. The heat storage capacity of DHN joins in the power and heat dispatch with higher flexibility. Next, three case studies have been tested and their results are discussed. Test results show that the proposed method is efficient and can significantly reduce the net operating cost.

Some conclusions of this chapter are summarized as below:

- 1) Considering the specific model of DHN breaks the space limitations of thermal transmission and encourages more dispatching flexibility of working units in MEMG.
- 2) Based on the transmission delay and the high inertia property of heat energy, DHN can be utilized as an HST with limited capacity, participating in the units dispatching of MEMG.
- 3) Integrating the power and heat networks can introduce more scheduling flexibility to the MEMG as well as reduce the overall operating cost.

The above conclusions can be valuable references for the optimal operation problem of MEMG.

Chapter 5 Optimally Coordinated Dispatch of MEMG with Demand Response

5.1 Introduction

In a traditional energy system, diverse energy resources such as electricity, heat, and gas are usually treated and supplied separately, which leads to low energy utilization efficiency. The multi-energy microgrid is then introduced to address the efficient utilization of diverse energy resources so as to meet different types of energy requirements and improve the living quality for customers [38-40]. In practice, a MEMG usually consists of many kinds of working units to simultaneously provide electricity and thermal energy supply to consumers. Nowadays, due to the different technical limits and operational characteristics of these units, how to develop appropriate methods to dispatch and schedule them in order to improve the energy utilization efficiency and economic benefits has captured a large amount of researchers' attention [41]. Furthermore, the investigation on the interaction and coordination between different types of energies has become another key topic in terms of microgrids [42].

In the meantime, the ever-growing electric and heat demands add a significant challenging dimension to the operation of MEMG. there are installed capacity limits to what can be achieved on the supply side, which may sometimes lead to the unbalance of supply and needs [33]. Demand response management plays a pivotal role to achieve supply-demand balance by taking advantage of the load flexibility and reshaping the load profile [43]. The ongoing researches [34, 44-46] also illustrate that day-ahead demand response strategies can significantly increase the economic performance of the electrical network. However, DRM (especially the thermal demand response) is not widely considered in the coupled electric and heat networks.

In this chapter an optimal operation approach of a MEMG considering DRM is proposed. The objective of this method is to minimize the total daily cost of the system while satisfying all the system technical constraints. The main contents of this chapter are summarized as follows:

- 1) The specific model of DRM including electrical demand response (PBDR strategy) and thermal demand response (ITC strategy) is systematically built, which can be integrated into MEMG's operation.
- 2) A novel combined heat and power microgrid optimal dispatching strategy is proposed, which coordinated the day-ahead PBDR management and the ITC strategy, in order to enhance the system's technical, economic performance.
- 3) The entire problem is linearized into a mixed-integer linear programming (MILP) model which can be efficiently solved. Apart from that, three relative case studies are designed and compared to the presented model. Simulation results show that the proposed method outperforms non-coordinated approaches or traditional methods without demand response in terms of operating costs.

5.2 Demand Response Management (DRM)

5.2.1 Introduction to DRM

With the development of the communication system and electrical technology, the smart grid becomes the future trend of the power system [47]. Conducting DRM is one of the features of the smart grid. DRM can help customers consume energy in a more efficient and cost-saving way based on their own intention. Usually, DRM is the first choice when energy policy decisions are being made, because it can create mutual benefits for both customers and power companies [48]. Further, due to the random property of RES, the imbalance issue between generation and consumption in the power system becomes more

and more obvious. DRM is also playing an important role in overcoming this kind of problem [49].

The smart grid vision is to encourage consumers to actively participate in power system generation and consumption. On the other hand, smart meters can collect detailed data from end-users and can conduct automatic control for home appliances, which lay a solid foundation for the promotion of DRM. Besides, it is revealed by some studies that smart buildings have great potential to implement DRM [50, 51].

The concept of DRM is that consumers adjust their energy consumption according to the electricity price or incentives. From a different point of view, DRM can be designed differently [52]. For example, from the perspectives of the electricity market, DRM is designed to reduce the generation cost, increase the capacity of energy reserves through smart responses. From the view of the environment, DRM can improve energy efficiency and reduce greenhouse gas emissions, thus environmental goals can be achieved.

DRM is usually divided into the following two types:

- 1) Price-based DR: Consumers adjust their electrical demands according to the variation of electricity price, which contains time of use (TOU) pricing, real-time (RTP) pricing, critical peak pricing (CPP), etc. Users who want to participate in this kind of DRM scheme can sign relative pricing contracts with power companies.
- 2) Incentive-based DR: Power companies make deterministic or time-varying policies to motivate consumers to respond and reduce demands when system reliability is affected or emergency incidents occur. This kind of DRM includes direct load control (DLC), interruptible load (IL), demand-side bidding (DSB), emergency demand response program (EDRP) and capacity/ancillary service program (CASP).

5.2.2 Price-based Demand Response (PBDR) Modelling

In order to better match the supply with need in the power network, PBDR has been widely applied for its benefits of enhancing the economic performance of the electricity market [53]. In PBDR management, the electricity price for the next day is sent to the consumers 24 hours ahead. Based on this information, consumers will adjust their electrical demands. For instance, it is assumed that end-users would use more electricity in a lower electrical price period, and vice versa. According to reference [8], the relationship between electrical price $P_{pr,t}$ and load demands $P_{load,i,t}$ can be modelled as:

$$P_{load,i,t} = BC_{pr,t}^{\varepsilon} \quad (5.1)$$

Reference [54] discusses how to calculate parameters A and ε .

According to the data used in [45], a power price elasticity of -0.2122 is applied in this study. In order to conduct the PBDR model with efficiency, 10 price level rates are predefined, which can be found in the Table. 5-1.

Table 5-1. Simulation results

PBDR levels	Price Rate (%)	Expected Response rates (%)
1	70	107.9
2	80	104.8
3	90	102.3
4	100	100.0
5	110	98.0
6	120	96.2
7	130	94.6
8	140	93.1
9	150	91.8
10	160	90.5

Based on the above-mentioned PBDR levels, the consumers' electrical demands can respond accordingly. Actual power demands with PBDR strategy can be calculated by the following equations:

$$P_{load,i,t} = \sum_{j \in J} \delta_j l_j^{level} P_{load,i,t}^o, \forall t \in T \quad (5.2)$$

$$Q_{load,i,t} = \sum_{j \in J} \delta_j l_j^{level} Q_{load,i,t}^o, \forall t \in T \quad (5.3)$$

where j is the PBDR level and J denotes the sets of all PBDR levels. $P_{load,i,t}$ and $Q_{load,i,t}$ are the active/reactive power at node i with PBDR strategy respectively; $P_{load,i,t}^o$ and $Q_{load,i,t}^o$ are the original active/reactive power at node i without PBDR strategy respectively; δ_j indicates the binary on/off decision of PBDR level ($\delta_j = 1$ means the price is at j level and vice versa); l_j^{level} is the load demand response rate of level j .

5.2.3 Indoor Temperature Control (ITC) Modelling

The thermal power generated by CHPs and EBs would enter the primary supply pipes to meet the heat requirement. This process can be described as (5.4)-(5.5).

$$H_{s,k,t}^+ - H_{r,k,t}^- = (H_{CHP,t} + H_{EB,t}) \cdot \eta_{hexl}, \quad k \in K_{hs}, t \in T \quad (5.4)$$

$$m_{s,k,t} = m_{r,k,t}, \forall k \in K_{hs}, t \in T \quad (5.5)$$

Heat loads are the quantity of heating energy that must be used to warm buildings so as to keep people comfortable. In this chapter, indoor temperature-dependent heat loads control is utilized. In this model, the design heat demands are related to the indoor and outdoor ambient temperature. Fig. 5-1 depicts the heat conduction effects of a building.

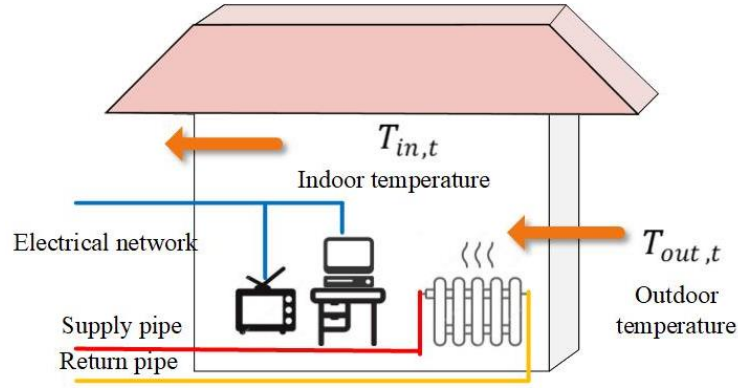


Figure 5-1. Heat conduction through building shells.

The outdoor temperature affects the indoor temperature by thermal conduction through building shells, including roofs, walls, doors, windows, etc. It is assumed that all the buildings are of the same type for simplicity. The thermal conduction equation for a building can be expressed as follow:

$$H_{b,t}^T = H_{s,b,t}^T / \tau = (T_{am,t} - T_{in,b,t}) / R_T, \quad \forall b \in B, t \in T \quad (5.6)$$

According to (5.6), a time-varying heat conduction model is formulated in Eq. (5.7). This equation demonstrates that the indoor heat energy variation in a building is the result of a combination of heat conduction from the outdoor environment and thermal power obtained from DHN. It is then linearized to a state model and formulated as (5.8). Next, in order to guarantee customers' benefits, the design heat demands $H_{b,t}^{load}$ are calculated with the potential minimal heat energy provided, formulated as (5.9). The relationship between internal thermal power in heat pipes and customers' heat demands are (5.10)–(5.11). Note that some factors like customer behavior and residence thermal comfort may have effects on the indoor temperature at the building and room level. In this regard, Ref. [55] presents a complete indoor temperature model, which considers consumer behavior and the customer's thermal comfort lifestyle for a building.

However, this thesis focuses on the whole system and network-level coordinated dispatch of electricity and heat, therefore such residential behavior effects can be

neglected as compared with the effects from DHN and outdoor environment [34]. Integrating such human behavior impacts the problem modeling may be a future direction for research work in this area.

$$C_{air}(dT_{in,b,t}/dt) = H_{ra,b,t} \cdot \eta_{ra} + H_{b,t}^T, \quad \forall b \in B, t \in T \quad (5.7)$$

$$C_{air}(T_{in,b,t} - T_{in,b,t-1})/\tau = H_{ra,b,t} \cdot \eta_{ra} + H_{b,t}^T, \quad \forall b \in B, t \in T \quad (5.8)$$

$$H_{b,t}^{load} = (T_{in,b,t}^{\min} - T_{am,t})\Delta t / R_t, t \in T \quad (5.9)$$

$$H_{s,k,t}^- - H_{s,k,t}^+ = H_{b,t}^{load}, k \in K_{hl}, t \in T \quad (5.10)$$

$$m_{s,k,t} = m_{r,k,t}, \forall k \in K_{hl}, t \in T \quad (5.11)$$

It is worth to mention that by applying a temperature-dependent heat loads control strategy, the heat energy requirement becomes flexible. This is mainly because that the indoor temperature usually fluctuates within a certain range to make dwellers comfortable. As a result, the heat loads can be controlled in a range corresponding to the variable temperature.

5.3 Coordinated Operation Method Considering DRM

5.3.1 Objective Function

The structure of a CCHP-based multi-energy microgrid (MEMG) in this paper is the same as Fig.1-2. Similar to Chapter 4, In the MEMG operation, the objective is to minimize the daily net operation cost C_{total} while satisfying all the constraints of the components and the whole system. The total cost includes fuel cost $C_{f,t}$ of CHP plants, start-up/shut-down cost $C_{st,t}/C_{sd,t}$, operation & maintenance (O&M) cost $C_{om,t}$ of all the units, exchange cost with utility grid $C_{e,t}$, as well as the revenue of selling heat to consumers $C_{s,t}$.

$$MINC_{total} = \sum_{t=1}^T (C_{f,t} + C_{e,t} + C_{st,t} + C_{sd,t} + C_{om,t} - C_{s,t}) \Delta t \quad (5.12)$$

$$C_{f,t} = C_{gas} \cdot \left[\left(P_{CHP,t} / \eta_{CHP} \right) \cdot \Delta t / L_{HVNG} \right] \quad (5.13)$$

$$C_{e,t} = C_{pr,t} \cdot (P_{gd,t} + P_{sd,t}) \Delta t \quad (5.14)$$

$$C_{st,t} = \max \left\{ 0, U_{CHP,t}^i - U_{CHP,t-1}^i \right\} \cdot C_{CHP}^{st} + \max \left\{ 0, U_{EB,t}^i - U_{EB,t-1}^i \right\} \cdot C_{EB}^{st} \quad (5.15)$$

$$C_{sd,t} = \max \left\{ 0, U_{CHP,t-1}^i - U_{CHP,t}^i \right\} \cdot C_{CHP}^{sd} + \max \left\{ 0, U_{EB,t-1}^i - U_{EB,t}^i \right\} \cdot C_{EB}^{sd} \quad (5.16)$$

$$C_{s,t} = \sum_{b \in B} (C_{H,t} H_{b,t}^{load}) \cdot \Delta t \quad (5.17)$$

$$C_{om,t} = C_u^{om} \cdot \left(\sum_{i \in I} P_{u,t}^i \right) \Delta t \quad (5.18)$$

5.3.2 Constraints

1) Constraints for DG and Auxiliary units

As mentioned before, the generation output of each DG (WT, PV, CHP) and ancillary device (EB) should be within its technical limits, and the incremental change of the units within a single period is limited by its ramping capability. These constraints can be expressed as:

$$P_{CHP}^{MIN} \leq P_{CHP,t}^i \leq P_{CHP}^{MAX} \quad (5.19)$$

$$-R_{CHP}^{down} \Delta t \leq P_{CHP,t}^i - P_{CHP,t-1}^i \leq R_{CHP}^{up} \Delta t \quad (5.20)$$

$$P_{WT}^{MIN} \leq P_{WT,t}^i \leq P_{WT}^{MAX} \quad (5.21)$$

$$-R_{WT}^{down} \Delta t \leq P_{WT,t}^i - P_{WT,t-1}^i \leq R_{WT}^{up} \Delta t \quad (5.22)$$

$$P_{PV}^{MIN} \leq P_{PV,t}^i \leq P_{PV}^{MAX} \quad (5.23)$$

$$-R_{PV}^{down} \Delta t \leq P_{PV,t}^i - P_{PV,t-1}^i \leq R_{PV}^{up} \Delta t \quad (5.24)$$

$$P_{EB}^{MIN} \leq P_{EB,t}^i \leq P_{EB}^{MAX} \quad (5.25)$$

$$-R_{EB}^{down} \Delta t \leq P_{EB,t}^i - P_{EB,t-1}^i \leq R_{EB}^{up} \Delta t \quad (5.26)$$

where P^{min}/P^{max} , are the minimum/maximum power output of each unit; R^{down}/R^{up} are the maximum ramp down/up rate of each component.

2) Constraints for ES

As for the ES units, state limit, charging/discharging power constraints, the energy limit should be satisfied. Similar to Chapter 4, since DHN can be seen as an HST, we only consider EES in this study.

$$0 \leq P_{EES,t}^{ch,i} \leq U_{EES,t}^{ch,i} \cdot P_{ESC}^{MAX} \quad (5.27)$$

$$0 \leq P_{EES,t}^{dis,i} \leq U_{EES,t}^{dis,i} \cdot P_{EES,t}^{dis} \quad (5.28)$$

$$\mu_{EES}^{MIN} \cdot E_{EES}^{cap} \leq E_{EES,t}^i \leq \mu_{EES}^{MAX} \cdot E_{EES}^{cap} \quad (5.29)$$

$$U_{EES,t}^{ch,i} + U_{EES,t}^{dis,i} \leq 1 \quad (5.30)$$

$$E_{EES,0}^i = E_{EES,N\Delta t}^i \quad (5.31)$$

Equation (5.31) illustrates that the electric energy stored in EES at the beginning of the day should be equal to the energy stored at the end of the day.

3) Distribution Power Flow Constraints

MEMG must firstly satisfy the distribution network power flow constraints [56], which can be formulated as follows.

$$P_{i+1,t} = P_{i,t} + P_{G,i,t} - P_{load,i,t} \quad (5.32)$$

$$Q_{i+1,t} = Q_{i,t} + Q_{G,i,t} - Q_{load,i,t} \quad (5.33)$$

$$V_{i+1,t} = V_{i,t} - \frac{r_i P_{i,t} + x_i Q_{i,t}}{V_0} \quad (5.34)$$

$$1 - \Delta V_{\max} \leq V_{i,t} \leq 1 + \Delta V_{\max} \quad (5.35)$$

$$P_{G,i,t} = \sum_{i \in I} P_{MT,t}^i + \sum_{i \in I} P_{WT,t}^i + \sum_{i \in I} P_{PV,t}^i + \sum_{i \in I} (P_{EES,t}^{dis,i} + P_{EES,t}^{ch,i}) - \sum_{i \in I} P_{EB,t}^i \quad (5.36)$$

$$-P_{\max} \leq P_{i,t} \leq P_{\max} \quad (5.37)$$

$$-Q_{\max} \leq Q_{i,t} \leq Q_{\max} \quad (5.38)$$

4) DHN Constraints

To protect the thermal pipes, their inside temperature should be in a range as:

$$T_s^{\min} \leq T_{s,k,t}^+ \leq T_s^{\max}, \forall k \in K_{ps}, t \in T \quad (5.39)$$

$$T_s^{\min} \leq T_{s,k,t}^- \leq T_s^{\max}, \forall k \in K_{ps}, t \in T \quad (5.40)$$

$$T_r^{\min} \leq T_{r,k,t}^+ \leq T_r^{\max}, \forall k \in K_{pr}, t \in T \quad (5.41)$$

$$T_r^{\min} \leq T_{r,k,t}^- \leq T_r^{\max}, \forall k \in K_{pr}, t \in T \quad (5.42)$$

Besides, to make sure customers feel comfortable, the indoor temperature of each building should also be maintained within a suitable range:

$$T_{in,b,t} \geq T_{in,b,t}^{\min}, \forall b \in B, t \in T \quad (5.43)$$

$$T_{in,b,t} \leq T_{in,b,t}^{\max}, \forall b \in B, t \in T \quad (5.44)$$

Other constraints of heat networks are listed in (3.1) to (3.26).

5.3.3 Model Linearization

It is obvious that the start-up/shut-down cost functions (5.15) and (5.16)) are nonlinear equations. Thus, the proposed models are formulated as the mixed-integer nonlinear programming problems, which is time-consuming and may need massive calculation. To solve this problem, the start-up and shut down costs are linearized as follows [30]:

$$\begin{cases} C_{st,t} \geq 0 \\ C_{st,t} \geq (U_{CHP,t}^i - U_{CHP,t-1}^i) \cdot C_{CHP}^{st} + (U_{EB,t}^i - U_{EB,t-1}^i) C_{EB}^{st} \end{cases} \quad (5.45)$$

$$\begin{cases} C_{sd,t} \geq 0 \\ C_{sd,t} \geq (U_{CHP,t-1}^i - U_{CHP,t}^i) \cdot C_{CHP}^{st} + (U_{EB,t-1}^i - U_{EB,t}^i) C_{EB}^{st} \end{cases} \quad (5.46)$$

After the linearization, the proposed model can be converted to a MILP problem. Besides, a step-by-step flowchart is shown in Fig. 5-2 to demonstrate the whole solution process of the proposed method.

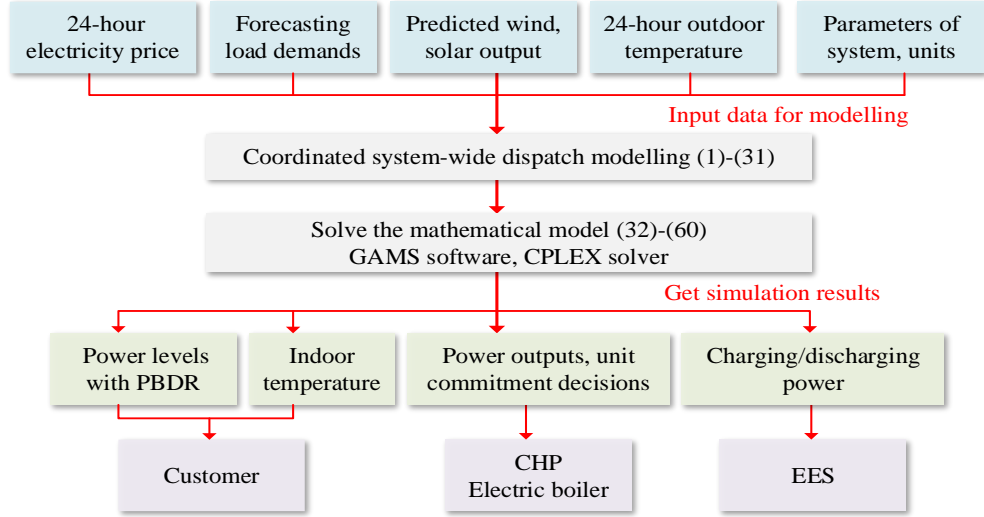


Figure 5-2. Flowchart of the proposed method.

5.4 Simulation

5.4.1 Tested Systems

The test is conducted on two MEMGs with coupled heat and electrical networks. The first one is based on the IEEE 33-bus radial distribution network [45] and a 13-pipe DHN. The second simulation is conducted on a larger MEMG to show the performance and scalability of the proposed framework, with IEEE 69-bus radial system and a 29-pipe DHN. In both of these systems, V_0 is 1.0 p.u. and ΔV_{\max} are set to be $\pm 5\%$ of the nominal level [56].

1) 33-bus MEMG

There are three heat sources in this area in this smaller system, which are connected to buses 6, 17 and 32 respectively. It is assumed that each heat node has 150 demand units. Table.5-2 shows the location of each generation and auxiliary unit in 33-bus MEMG, and the whole diagram of 33-bus MEMG is shown in Fig. 5-3.

Table 5-2. Location of each unit in 33-bus MEMG

Component	Location in EN	Location in DHN
PV	Bus4, Bus9, Bus26	/
WT	Bus4, Bus23	/
EES	Bus6, Bus23	/
CHP	Bus6, Bus32, Bus17	Node1, Node6, Node9
EB	Bus17, Bus32	Node6, Node9

In accordance with practical scheduling, the time interval of the case studies is set to 1 hour and the total time horizon T is set to be 24 hours.

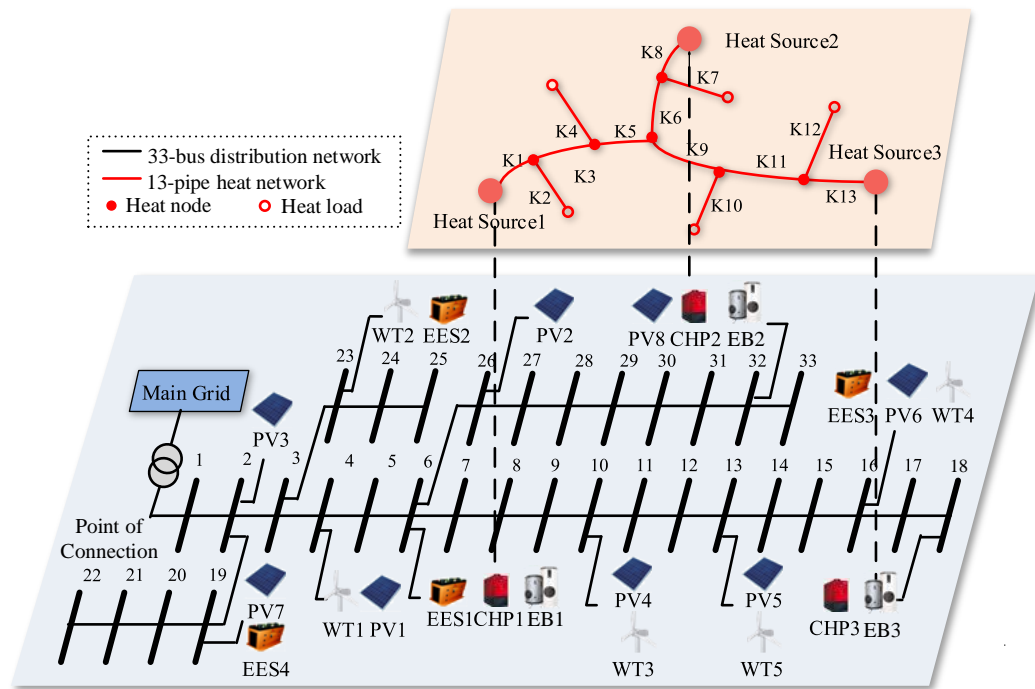


Figure 5-3. Schematic diagram of 33-bus MEMG.

Note that the uncertainty of renewable generators, loads, as well as electricity price, is not discussed in this chapter and we assume that the renewable power outputs can be obtained from forecasting [57, 58].

It is assumed that all loads in this MEMG can be adjusted according to the PBDR and indoor ambient temperature control. The day-ahead market electricity price for each hour can be found in Fig. 5-3 [8]. Other data are collected from references [7, 11, 14] and then modified with some practical considerations. It must be noted that any reasonable data can also be used and would not have effects on the effectiveness of the proposed approach.

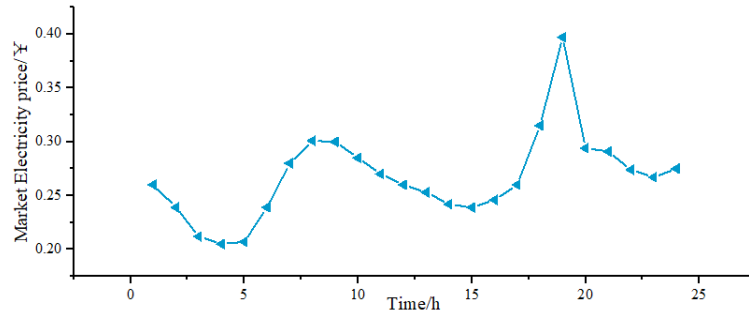


Figure 5-4. Day-ahead 24h power transaction price.

Parameters of EES are shown in Table.5-3, while the parameters of DHN are listed in Table.5-4. Table. 5-5 presents the parameters of working units in this tested system. The mass flow rate in heat pipes is the same as in the last chapter.

Table 5-3. EES Parameters

Name	Value	Name	Value	Name	Value
μ_{ES}^{MIN}	0.15	μ_{ES}^{MAX}	1.0	C_{ES}^{om}	0.073¥/kW
E_{ES}^{cap}	800kWh	$\eta_{ESC/ESD}$	0.8	α_{ES}	0.001
P_{ESC}^{MAX}	250kW	P_{ESD}^{MAX}	250kW	$E_{EES,0}$	400kWh

Table 5-4. DHN Parameters

Name	Value	Name	Value	Name	Value
ρ	1000kg/m ³	C^{air}	0.53kWh/°C	η_{hex1}	0.9
η_{ra}	0.9	R_T	2.8°C/kW	C_H	0.1

$T_{in,b,t}^{max}$	22	$T_{in,b,t}^{min}$	18	η_{CHP}	0.3
η_h	0.85	η_L	0.15		

Table 5-5. Units Parameters

Type	C_{om}	P^{max}	P^{min}	R^{down}	R^{up}	C^{st}	C^{sd}
CHP	0.0990¥/kW	1000 kW	200 kW	5kW/min	10kW/min	1.94¥	1.82¥
Photovoltaic cell	0.0133¥/kW	300 kW	0 kW	/	/	/	/
Wind turbine	0.0145¥/kW	350 kW	0 kW	/	/	/	/
Electric boiler	0.0089¥/kW	300 kW	0 kW	2kW/min	3kW/min	1.32¥	1.15¥

2) 33-bus MEMG

In order to discuss the stability of this method, an IEEE 69-bus radial distribution system with coupled 27-pipe DHN is tested, as shown in Fig. 5-5. The capacities of the units in this system are the same as the 33-bus system. The configuration of these two systems is summarized in Table 5-6.

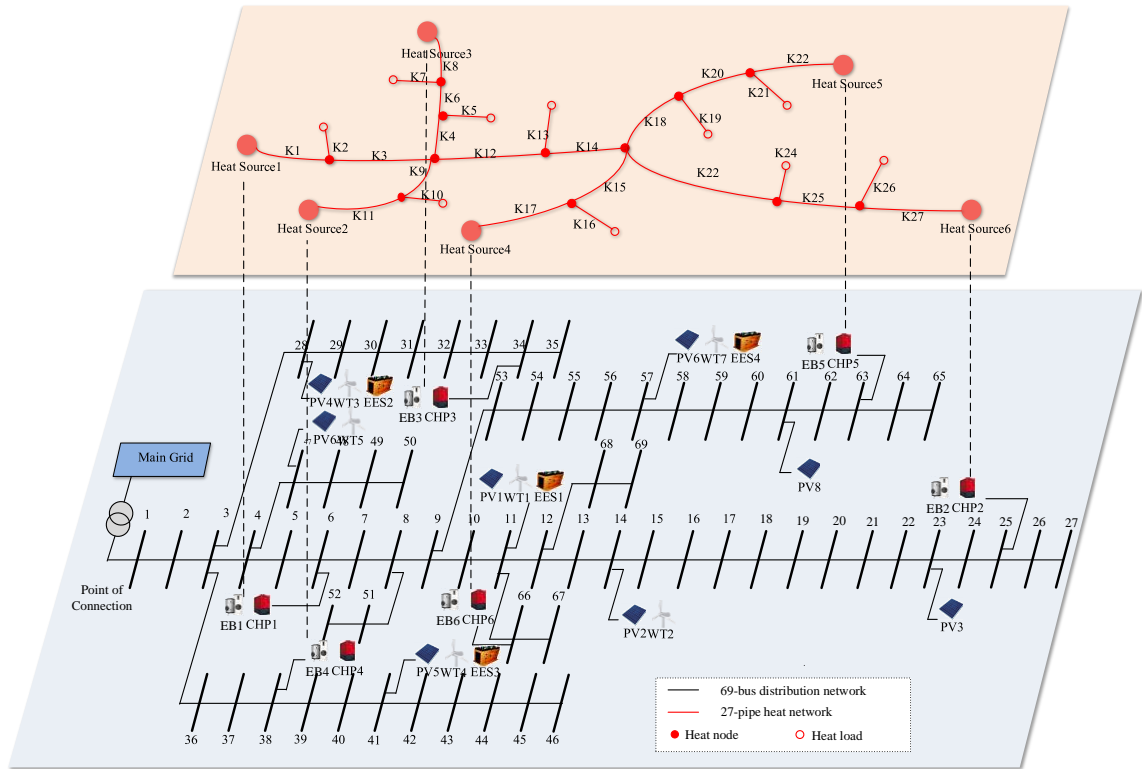


Figure 5-5. Schematic diagram of 69-bus MEMG.

Table 5-6. Configuration of the tested systems

		Test System	
		33-bus MEMG	69-bus MEMG
<i>Electrical power network</i>	bus	33	69
	Line	32	68
	WT	5	6
	PV	8	8
<i>DHN</i>	EES	3	4
	node	6	14
	pipe	13	29
	load	5	10
	CHP	3	6
	EB	6	6

5.4.2 Results and Discussion

3 case studies are designed in order to verify the effectiveness and benefits of the proposed method.

Case1 is an ordinary case without consideration of the specific model of DHN and demand response management is not applied. **Case2** considers the DHN constraints and **Case3** is the proposed method. All the three cases are conducted on both 33-bus MEMG as well as 69-bus MEMG to show the scalability of the proposed method. Again, the simulation is conducted on GAMS software, which has been commonly used for solving the MILP problems.

1) Results for 33-bus MEMG

The electric demand profiles with and without demand response strategies are shown in Fig.5-6. During 11:00-13:00 and 17:00-21:00 electric load reach to its peak, while load valley usually appears around 1:00-4:00 since most consumers are sleeping. After implementing PBDR strategy, power loads increase a little bit during 0:00-6:00 and 14:00-16:00. On the other hand, customers would reduce their demands between 7:00-

11:00 and 19:00-22:00 to adjust the high price. Thus, in the sense of power system operation, the variation of electric loads is mitigated with the implementation of PBDR.

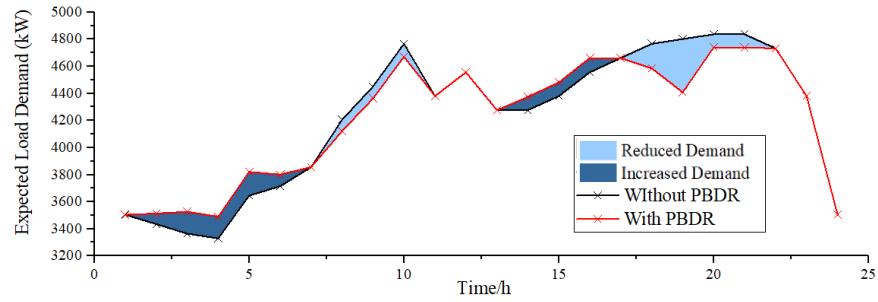
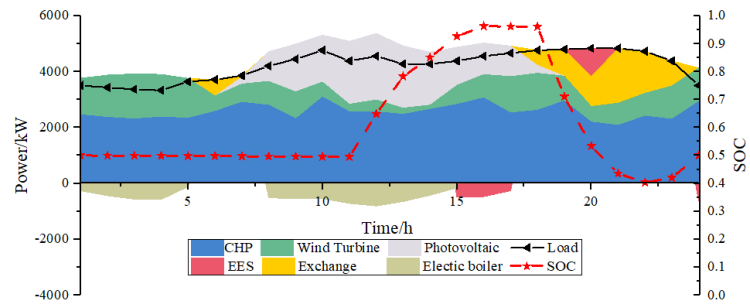
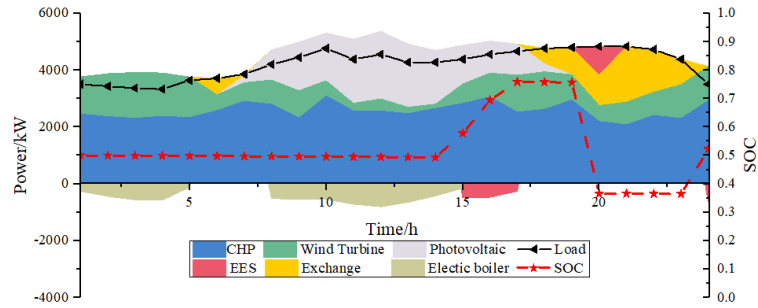


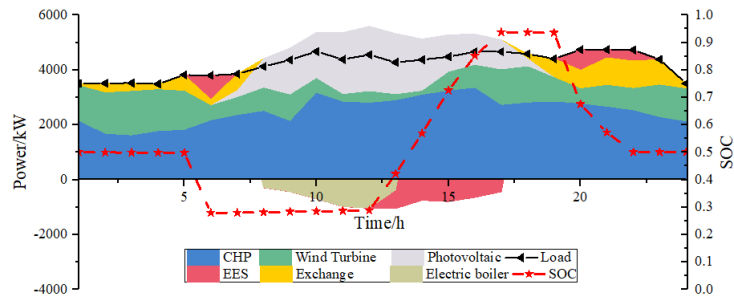
Figure 5-6. Electric load profile.



(a)



(b)



(c)

Figure 5-7. Power balance in 33-bus MEMG. (a) Case1. (b) Case2. (c) Case3.

Fig.5-7 presents the power condition under Case1, Case2, and Case3 respectively. It is indicated in the figure that the power demands can be met without any shortage in all the cases. All the components in the tested MEMG are optimally dispatched based on their constraints, which means that the proposed method is effective in the aspect of EN.

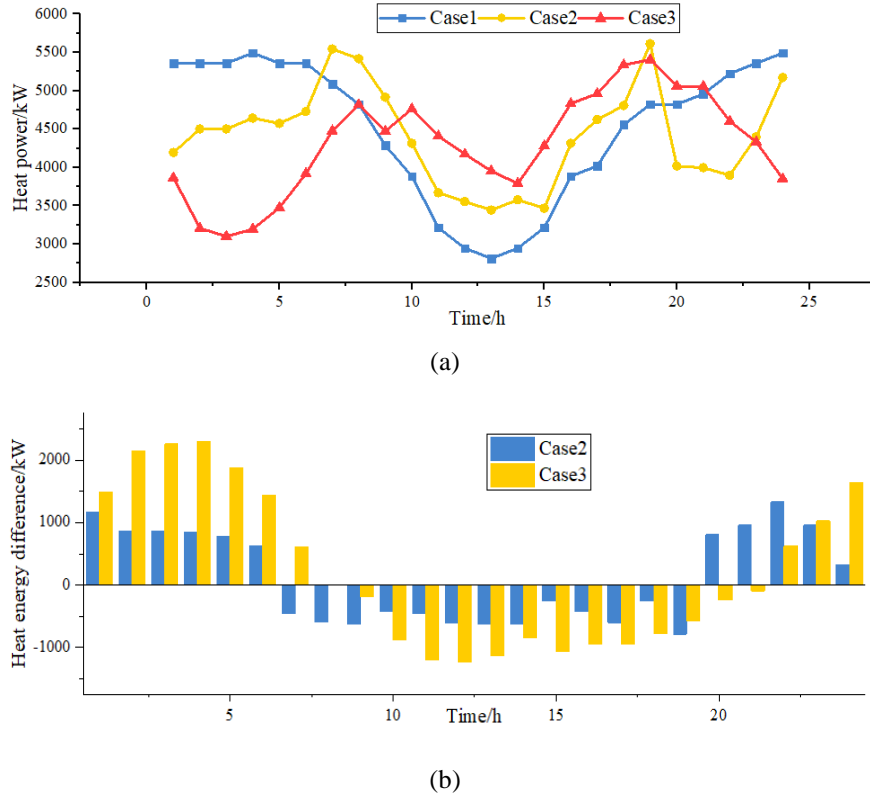


Figure 5-8. Simulation Results of Heat Power.

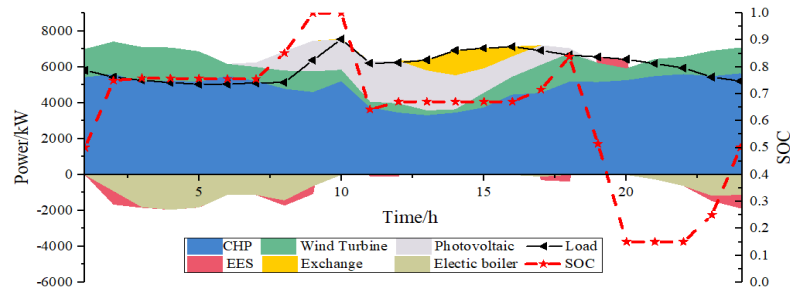
(a) Comparisons of heat power generation among Case1-3. (b) Storage status of DHN.

Fig.5-8 (a) shows the total heat generation of CHP units and EB units. Just as discussed in the last chapter, DHN can be seen as an HST, thus in Case2 and Case3 heat generation does not balance the demands at each hour. For example, during 0:00-5:00 in the morning, the required heat load is high due to the low outdoor temperature, but the electric demand is low because most of the customers are sleeping. For example, during 10:00-20:00 periods, the electric demand gradually reaches to its peak, the total heat output will become larger in order to meet the requirement. Whereas at the same time, the extra generated heat will be stored in the heat pipes, resulting in a higher temperature of water

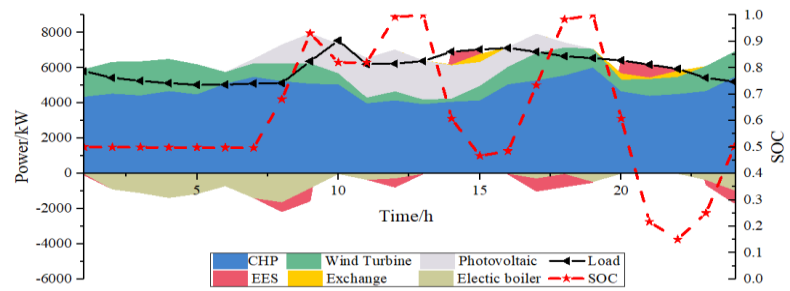
inside the thermal pipes. The heat difference between thermal generation and demand during 24h is shown in Fig.5-8 (b). Apart from that, compared to Case2 which does not consider DRM, heat generation in Case3 is more adjusted to the variation trend of power loads (Fig.5-6) after applying the ITC strategy. Therefore, it is indicated that in the proposed method, DHN and power network are strongly coupled, and applying DRM introduces more dispatching flexibility to MEMG.

2) Results for 69-bus MEMG

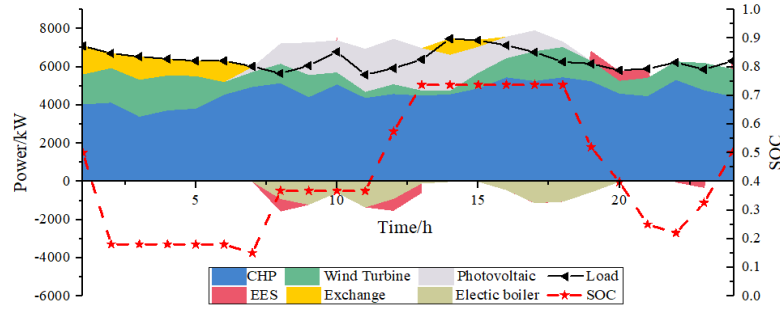
Fig. 5-9 shows the power balance conditions in the 69-bus system under 3 cases. Table 5-7 lists the total operational cost under all these cases. It can be found that in the proposed method, PBDR can help us to do load shifting. As a result, CHP power outputs decrease, thus the total operational cost can be reduced (9.3% less than case1). The results show that the implementation of DRM encourages more economic benefits in MEMG.



(a)



(b)



(c)

Figure 5-9. Power balance in 69-bus MEMG. (a) Case1. (b) Case2. (c) Case3.

Table 5-7. Total costs in 69-bus system

Items	Case1	Case2	Case3
Total cost	25335.82	24497.49	23151.80

It is worth to mention that the IEEE 33-bus system and 69-bus system are both standard benchmark test systems, which have been widely applied in MEMG's operation problems. The amount of variables of this problem is more than 10000 and the solution takes only 5.67 seconds and 20.34 seconds for these two systems respectively. Since the solution speed is very fast, it is scalable to larger systems. Some other reasonable data for a larger tested system can also be used, which would not affect its effectiveness.

5.5 Summary

This chapter develops an optimal coordinated dispatch method of MEMG with DRM, aiming at minimizing the net operating cost of the system. And then a comprehensive and practical model of combined heat and electrical network is established, in which the electrical network power flow constraints, the technical limits of different units, the dynamic operating constraints of DHN and demand response are considered.

Then, three case studies are compared to show the benefits of considering the specific model of DHN and applying DRM in MEMG.

Some conclusions of this chapter are summarized as below:

- 1) Considering characteristics of DHN could decouple the generation and consumption of heat energy and introduces more scheduling flexibly of generation units.
- 2) PBDR and indoor ambient temperature control strategy can be implemented in MEMG coordinated dispatching to improve the holistic economic, technical performance.
- 3) The proposed model can be efficiently solved for online application.

Chapter 6 Two-Stage Stochastic Operation of MEMG

6.1 Introduction

In order to increase system energy utilization efficacy, traditional microgrid moves towards multi-energy microgrid (MEMG) [2], in which different kinds of energy sectors (like gas, heat, and power) are highly coupled.

As discussed before, some researchers have done studies related to MEMG's operation at the component or system level [3, 5], but most of these researches are focusing on deterministic day-ahead operation (i.e., the uncertainties are not considered), which is not so practical for industry application.

It is revealed by some studies and reports [15, 17] that the randomness property of RES raises significant challenges for the day-ahead microgrid operation. To solve this problem, some reference [17-19] employs a two-stage stochastic optimization approach to handle the uncertainties from wind outputs. The above papers verify that the stochastic optimization method is effective in smoothing out the fluctuations from RES. Nevertheless, they are more focusing on the electrical network. Little attention is paid to the uncertainties in the multi-energy system.

This chapter aims to optimally coordinate all the units in a MEMG with coupled heat and electrical network, and integrate the uncertainties from RES, loads and electricity price into the microgrid operation model. Firstly, the diverse uncertainties are modeled, and then a two-stage stochastic optimization method is proposed: the on/off statuses of each unit and charging/ discharging power of energy storage tanks are optimized in the day-ahead stage since they need to be decided under uncertainties in advance. The power outputs of each generator are optimized in the intra-day stage, which acts as a recourse to complete the operational decisions. The problem is formulated as a mixed-integer

linear two-stage optimization model, so that it can be efficiently solved by some existing solvers.

6.2 Modelling of Uncertainties

6.2.1 Scenario Construction

The generation outputs of RES, electricity price and loads should be forecasted one day ahead when we are optimizing the operation of MEMG. However, it is quite difficult to predict them accurately. Thus, modeling the randomness appropriately becomes a prerequisite of MEMG's operation. In this paper, we assume that the random variation of RES generation follows the beta distribution [59].

The Beta distribution is formed with two shape parameters: α and β . The probability density function, mean and variance of Beta destruction for a forecasted power $P_{RES}^{t,i}$ can be expressed as:

$$f_{P_{RES}^{t,i}} = A \cdot P_{RES}^{t,i}{}^{\alpha-1} \cdot (1 - P_{RES}^{t,i})^{\beta-1} \quad (6.1)$$

Besides, we employ normal distribution to model the fluctuations of power loads and electricity price [60], which can be expressed as:

$$f_{P_{load}^{t,i}} = \frac{1}{\sqrt{2\pi}\sigma} \exp\left[-\frac{(P_{load}^{t,i} - \mu)^2}{2\sigma^2}\right] \quad (6.2)$$

Usually, we need to select suitable parameters in accordance with the actual conditions.

6.2.2 Scenario Reduction

In order to improve the computational efficiency, the number of scenarios should be reduced. In this chapter, a Simultaneous backward forward technique is utilized to choose a smaller number of scenarios to represent the original variation [61]. Let χ_s denotes scenario s ($s=1,2,\dots,N$), and the probability of χ_s happens is p_s . Then the distance between scenario pair (s, s') can be defined as:

$$D_{s,s'} = \max\{1, \|s - s^{av}\|, \|s' - s^{av}\|\} \|s - s'\| \quad (6.3)$$

where s^{av} denotes the average value of all the scenarios.

The scenario reduction method contains several steps as follow:

- 1) Let S be the set of all the initial scenarios, and S_d be the sets of scenarios that need to be deleted (initially null). Compare the distances between all the scenario pairs $D_{s,s'} = D(\chi_s, \chi_{s'})$, $(s, s' = 1, \dots, N)$;
- 2) For each scenario n , $D_n(r) = \min D_{n,s'}, n, s' \in S$ and $n \neq s'$. r is a scenario index, which means that it has the minimum distance with n .
- 3) Compute the probability $PD_n(r) = \sum_{u \neq n} p_u * D(\chi_n, \chi_u)$, $n \in S$. Choose d which satisfies $PD_d = \min PD_n, n \in S$.
- 4) $S = S - \{d\}$, $S_d = S_d + \{d\}$; $p_r = p_r + p_d$.
- 5) Repeat steps 2-4 until we get the ideal set S_i for computation.

6.3 Two-Stage Optimization Approach

Commitment decisions are assumed to be made in the first-stage (one day ahead) before the actual RES generation outputs, electricity price and loads profile are realized. These decisions should accommodate intra-day conditions. In the second stage, the intra-day

decisions like generation outputs of components are optimized after a realization of uncertainties. The two stages are linked with each other through system operational constraints. It is noted that charging and discharging power of EES are also determined in the first stage due to its strong time-coupling property. The solving flow chart of this problem can be seen in Fig. 6-1.

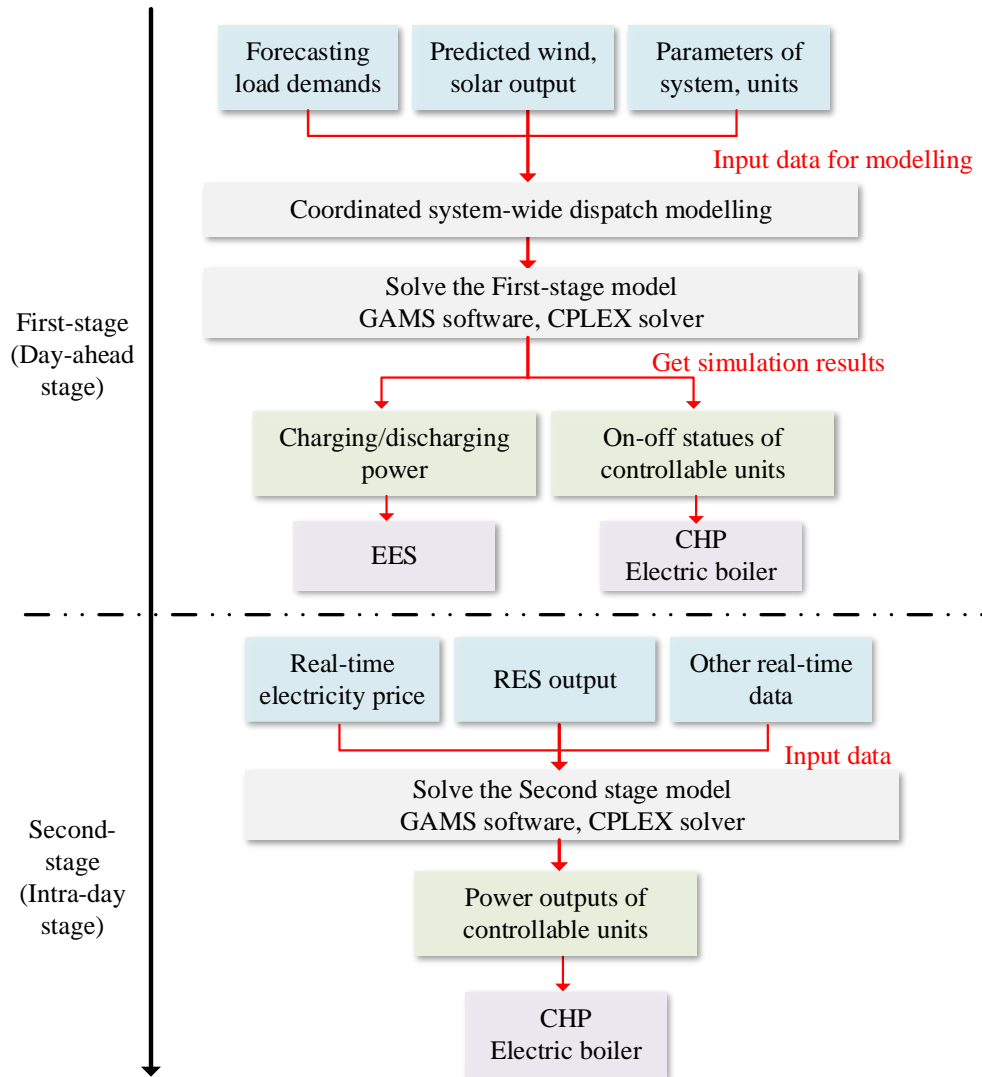


Figure 6-1. Flow chart of two-stage optimization approach

A general mathematical expression of the two-stage optimization model is [18]:

$$\min_{x \in F} \{f(x) + E(x, \omega)\} \quad (6.4)$$

where $f(x)$ is the first-stage (day-ahead) operation objective, x denotes day-ahead stochastic decisions sector; $E(x, \omega)$ is the expectation of second-stage (intra-day) operation objective, which is equal to $\min_{y \in \Omega(x, \omega)} L(y)$, where y denotes the second-stage decision vector and ω is the random vector.

Since we are using discrete scenarios, the above model can be formulated into a deterministic equivalence as:

$$\min_{x, y_1, y_2, \dots, y_s} f(x) + \sum_{s \in S_i} p_s L(y_s) \quad (6.5)$$

Equation (6.5) can be specifically expressed as:

$$\begin{aligned} \min C_{total} = & \left[\sum_{g \in G} \sum_{t \in T} (C_{g,t}^{SU} + C_{g,t}^{SD}) + \sum_{t \in T} (C_{EES,t}^{om} + C_{HST,t}^{om}) \right] \\ & + \sum_{s \in S_i} p_s \cdot \left[\sum_{g \in G} \sum_{t \in T} (C_{g,t}^{om}) + \sum_{t \in T} (C_{CHP,t}^f + C_t^{ex}) \right] \end{aligned} \quad (6.6)$$

In (6.6), The objective function consists of two parts: The first part includes the deterministic (decided by commitment decisions), start-up cost, shut-down cost of each controllable generator as well as the O&M cost of EES since these decisions should be made in advance. The second part is the expected operating, fuel cost as well as power exchange cost in the real-time stage.

6.4 Simulation and Discussion

6.4.1 Tested System

To verify the proposed two-stage stochastic approach, simulation studies have been carried out on a grid-connected MEMG which is based on the IEEE 33-bus distribution system, as shown in Fig. 6-2. It is assumed that there are both electrical load and heat

load existing at each bus. Due to the great loss of long-distance heat energy transferring, each heat load is supplied by the nearest CHP plant or EB.

The capacity and corresponding cost item of each generator are listed in Table 6-1. Parameters of EES and HST can be found in previous chapters.

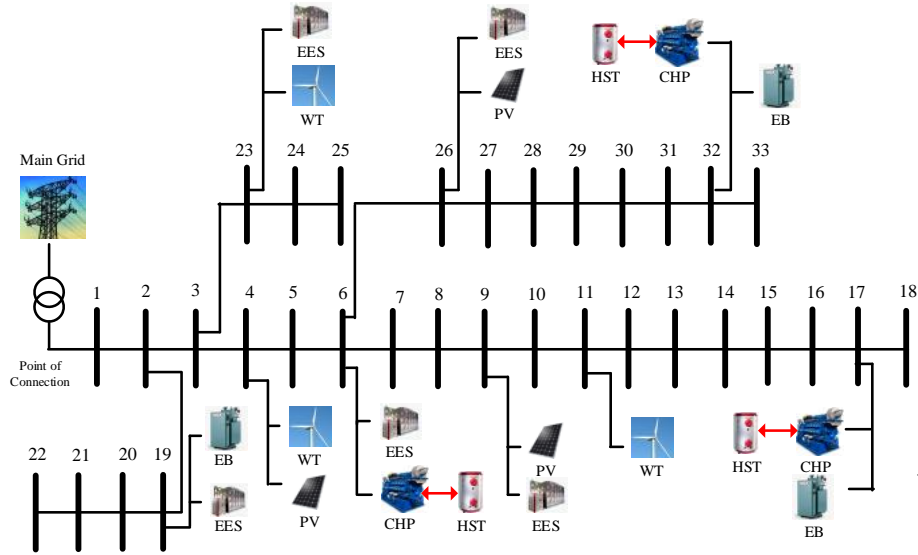


Figure 6-2. Flow chart of two-stage optimization approach

Table 6-1. Parameters of units

Type	C^{om}	P^{max}	P^{min}	R^{down}	R^{up}	C^{st}	C^{sd}
CHP	0.8700¥/kW	100kW	20 kW	5kW/min	10kW/min	1.94¥	1.82¥
PV	0.0133¥/kW	20 kW	0 kW	/	/	/	/
WT	0.0145¥/kW	55 kW	0 kW	/	/	/	/
EB	0.0089¥/kW	40 kW	0 kW	2kW/min	3kW/min	1.32¥	1.15¥

Besides, it is assumed that the variation of random electric/heat load and electricity price follows the normal distribution, where the mean value is the forecasted value and the standard deviation is set to be 4%. And the uncertainties from RES are assumed to follow the Beta distribution where α and β are set to 6.06 and 6.06 [62].

It is worth to mention that other reasonable data can also be used in the case study which would not affect the effectiveness of the proposed method. All the tests are run on an Intel(R) Core i5-7200U, 2.50-GHz personal computer with 8GB of memory. Scenario

construction and reduction are done on software Matlab 2017a, and the optimization problem is solved by a commercial software called GAMS (CPLEX solver).

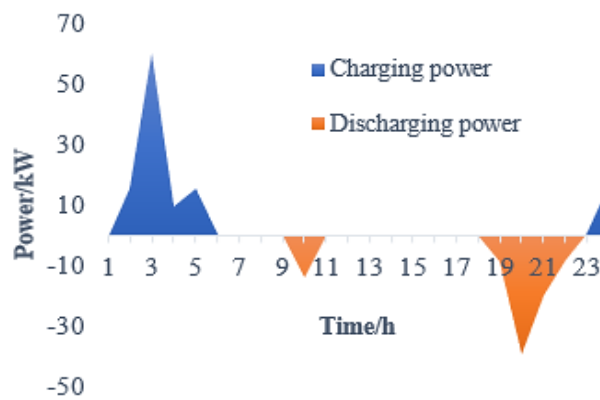
6.4.2 Simulation Results

1) Day-Ahead Operation (First Stage)

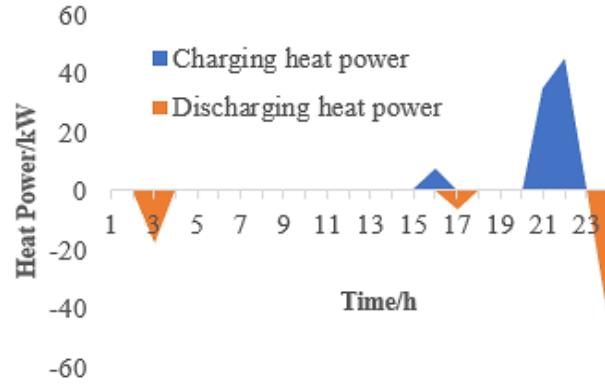
In the day-ahead stage, 1000 scenarios based on varies RES outputs, loads and electricity prices are randomly generated. And then 10 representative scenarios are selected with corresponding probabilities. The unit commitment results and charging/discharging power of EES and HST in the first-stage operation are shown in Table 6-2 and Fig. 6-3 respectively. The total expected operation cost of this stage is 5551.063¥.

Table 6-2. Unit commitment results

Type	Bus ID	Hour (1-24)
CHP	6	1 1
	17	1 1 0 0 1 1 1 1 1 1 1 1 1 1 1 1 0 1 1 1 1 1 1 1
	32	1 1 1 1 0 1 1 1 1 1 1 1 1 1 1 1 1 1 1 1 1 1 0 0
EB	17	0 0 0 1 1 1 1 1 1 0 0 0 0 0 0 0 0 0 0 0 0 0 0 0
	19	0 1 1 1 1 1 1 1 0 0 0 0 0 0 0 0 0 0 0 0 0 0 0 0
	32	0 0 1 1 1 1 1 1 0 0 0 0 0 0 0 0 0 0 0 0 0 0 0 0



(a)



(b)

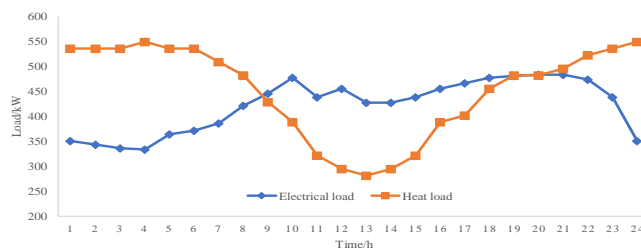
Figure 6-3. Charging/discharging power of (a) EES. (b)HST.

It is worth to mention that peak power demand appears at night (time period 18-22) whereas peak thermal demand appears in early morning (time period 0-6). It can be seen from Table 6-2 that EBs run during time period 2-7. This is reasonable because electric loads are relatively low during this period, surplus electricity can be used to generate heat energy. At the same time, EES store electricity while HST release heat energy to satisfy the customers' high thermal demands.

Besides, with the help of the CPLEX solver, the computation time is only 2.9 minutes. Which means that this method is suitable for doing practical day-ahead decisions.

2) Intra-Day Operation (Second Stage)

The intra-day operation is simulated based on the online hourly-ahead forecasts of RES generation, electrical/heat loads, and electricity price. The specified electrical/heat load, RES generation as well as electricity price are shown in Fig. 6-4.



(a)

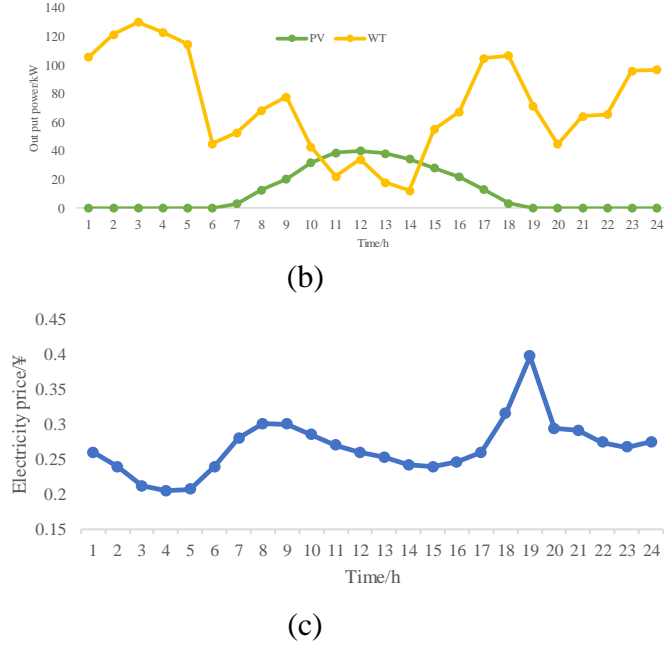
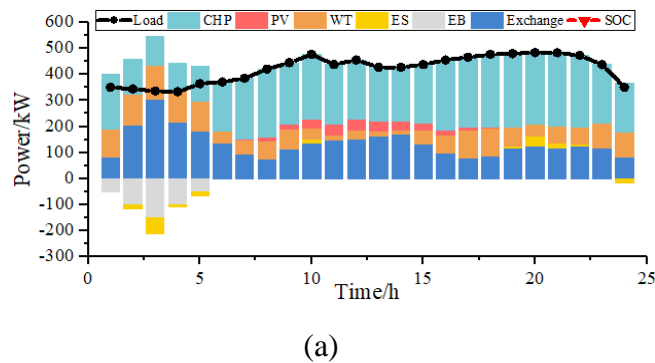
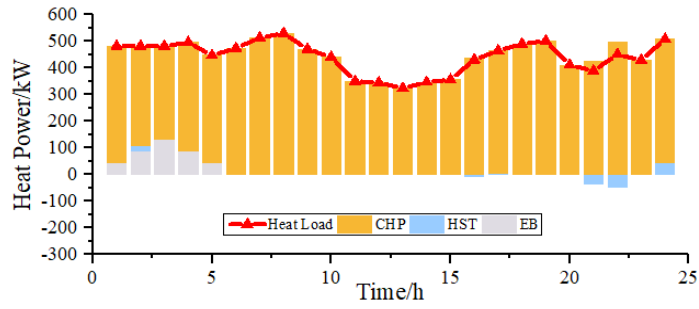


Figure 6-4. Specified input data for the second stage. (a)Load. (b) RES generation. (c) Electricity price.

With the above-specified data, the operation results in the second stage are shown in Fig. 6-5. And the total cost of the second stage is 5510.299¥.

In Fig.6-5, both heat and electrical load can be satisfied without any shortage in the second stage, which means that the proposed method is efficient in dispatching components in MEMG. Further, during time period 2-6, electricity price is kept at a low level, thus electricity is bought from the utility grid to charge EES and CHP plant reduces its generation outputs for higher economic performance. When the price is higher at the time period 18-23, the CHP plant produces more electricity, so that the power exchange cost can be decreased. At the same time, surplus heat energy generated by CHP will be stored in HST. Thus, it can be concluded that different energies are coordinated.





(b)

Figure 6-5. Operation results in the second stage. (a) Electricity balance condition. (b) Heat condition.

3) Feasibility check

In order to further demonstrate the benefits of our proposed method, a traditional single-stage deterministic optimization method (method 1) and single-stage stochastic optimization method (method 2) are also tested on the same MEMG. The total cost and voltage violation of three methods are listed in Table 6-3. It can be found that our method can achieve higher economic benefits and robustness of the whole system.

Table 6-3. Total cost and voltage violation

Item	Method 1	Method 2	Method 3 (proposed method)
Total cost (¥)	5230.140	5623.734	5510.299
Average voltage violation (%)	9.6%	0	0

6.5 Summary

This chapter proposes a two-stage stochastic operation approach of combined heat and electrical network. Firstly, the diverse randomness from RES generation, loads as well as electricity price is modeled and a large number of scenarios are generated. Then, the number of scenarios is reduced by the simultaneous backward forward technique. Finally, the effectiveness of the proposed method is tested on a MEMG, which is based on the IEEE 33-bus distribution system.

Some conclusions of this chapter are summarized as below:

- 1) The two-stage stochastic optimization method is efficient in solving MEMG's operation problem, considering the diverse randomness from RES, loads and electricity price.
- 2) The proposed method can effectively enhance the holistic economic viability and technical performance, which makes it a meaningful reference for the energy dispatch of combined heat and electrical network.

Chapter 7 Conclusions and Future Works

7.1 Conclusions

In this thesis, we addressed the optimal operation problem of multi-energy microgrid (MEMG) with coupled heat and electrical networks. One of the main contributions of our work is to formulate this task as a mix-integer linear programming optimization problem with constraints and to propose methods to solve it based on working units' characteristics and properties of different energy sectors.

A comprehensive model on different components in MEMG (including CHP, PV, WT, EB, ES) has been provided. The proposed model is mainly focused on their external characteristics and economic items, thus they can be applied in MEMG's operation problem.

The model of district heat network (DHN) has been presented. Our contribution here is twofold. First the nodal flow balance, mixing temperature constraints for DHN are systematically performed in the model, performed in the model, and second, the transmission delay and quasi-dynamics of DHN have been fully considered.

The focus of this thesis is on integrating heat and electrical network. Three new approaches are proposed to solve the optimal operation problem of MEMG. The first one takes both the constraints for the electrical network and DHN into consideration, thus DHN and electric power grids are highly coupled. Besides, DHN is seen as an HST joining in the power and heat dispatch with higher flexibility. In the second proposed method, we apply demand response management to shift the peak loads and to better operate the whole system. Thirdly, in order to integrate diverse uncertainties from RES, loads and electricity prices, a two-stage stochastic optimization approach is presented.

From a simulation point of view, our contribution lies in the comparison of the performance of proposed methods with other conventional operation techniques such as non-coordinated approaches or existing methods without demand response. All the proposed methods are performed on the IEEE 33-bus distribution system to test their effectiveness. Results show that our approaches obtain better results (higher energy utilization efficiency and less system operation costs).

7.2 Future Works

Many different possible works have been left for the future due to lack of time. Future works may include modeling other types of energy networks in MEMG, modeling more detailed thermal comfort and behaviors at the resident level, using more advanced solution algorithms as well as ensuring the security and resilience of MEMG.

Potential directions in this research area may contain the following ideas:

- 1) It could be interesting to consider other types of energy networks in MEMG. In this thesis, only electrical and DHN are considered and coupled. However, other kinds of energy sectors can also be integrated together by means of electric vehicles (EV), the power to gas units and so on. Modeling these energy networks in detailed and investigate their coordination with traditional electrical network may further enhance the overall economic benefits as well as energy utilization efficiency.
- 2) It is mentioned in **Chapter 4** that this thesis focuses on the whole system and network-level coordinated dispatch of electricity and heat, therefore such residential behavior effects can be neglected as compared with the effects from DHN and outdoor environment. Modeling more detailed thermal comfort and behaviors at the resident level may be a future direction for research work in this area.

- 3) The way the optimization problem is solved could be also changed: instead of using off-the-shelf software, it could be based on a more advanced solution algorithm, such as genetic algorithm (GA), simulated annealing (SA), etc.
- 4) Further, the proposed methods are all based on stable state MEMG, future work will consider dynamic system operation and modeling, and the stability, resilience assessment/enhancement of MEMG.

Author's Publication

- 1) **Y. Chen**, C. Dong, L.H.Koh, P.Wang et al., "Long-term optimization for the extension scheme of island microgrids," in 2018 13th IEEE Conference on Industrial Electronics and Applications (ICIEA), 2018: IEEE. (Published)
- 2) C. Zhang, Z. Dong, Y. Xu, and **Y. Chen**, "A two-stage robust operation approach for combined cooling, heat and power systems," in Energy Internet and Energy System Integration (EI2), 2017 IEEE Conference on, 2017, pp. 1-6: IEEE. (Published)
- 3) **Y. Chen**, Y. Xu, Z. Li, S. Feng, C. Hu, and K. L. Hai, "Optimally Coordinated Operation of a Multi-Energy Microgrid with Coupled Electrical and Heat Networks," in 2018 International Conference on Power System Technology (POWERCON), 2018, pp. 218-224: IEEE. (Published)
- 4) **Y. Chen**, Y. Xu, Z. Li, X. Feng. "Optimally Coordinated Dispatch of Combined-Heat-and-Electrical Network", IET Generation, Transmission & Distribution, 2019. (Published)
- 5) **Y. Chen**, Y. Xu, Z. Li, H. Yang, A. Verma, and LCP. da. Silva, "A Two-Stage Stochastic Operation Approach of Combined Heat and Power Networks," Proc. 9th IEEE Innovative Smart Grid Technologies-Asia (ISGT-Asia), China, May 2019. (Accepted)

Reference

1. Alahdad, Z., *Pakistan's energy sector: from crisis to crisis: breaking the chain*. 2012: Pakistan Institute of Development Economics.
2. Mancarella, P., *MES (multi-energy systems): An overview of concepts and evaluation models*. Energy, 2014. **65**: p. 1-17.
3. Smith, A.D. and P.J. Mago, *Effects of load-following operational methods on combined heat and power system efficiency*. Applied Energy, 2014. **115**: p. 337-351.
4. Fang, F., Q.H. Wang, and Y. Shi, *A novel optimal operational strategy for the CCHP system based on two operating modes*. IEEE Transactions on power systems, 2012. **27**(2): p. 1032-1041.
5. Wang, J., J. Sui, and H. Jin, *An improved operation strategy of combined cooling heating and power system following electrical load*. Energy, 2015. **85**: p. 654-666.
6. Lujano-Rojas, J.M., et al., *Optimizing Daily Operation of Battery Energy Storage Systems Under Real-Time Pricing Schemes*. IEEE Trans. Smart Grid, 2017. **8**(1): p. 316-330.
7. Li, Z. and Y. Xu, *Optimal coordinated energy dispatch of a multi-energy microgrid in grid-connected and islanded modes*. Applied Energy, 2018. **210**: p. 974-986.
8. Zhang, C., et al., *Robustly Coordinated Operation of A Multi-Energy Microgrid with Flexible Electric and Thermal Loads*. IEEE Transactions on Smart Grid, 2018.
9. Jiang, Q., M. Xue, and G. Geng, *Energy management of microgrid in grid-connected and stand-alone modes*. IEEE Trans. Power Syst, 2013. **28**(3): p. 3380-3389.
10. Yan, B., et al., *Operation and design optimization of microgrids with renewables*. IEEE Transactions on Automation Science and Engineering, 2017. **14**(2): p. 573-585.

11. Kanchev, H., et al., *Emission reduction and economical optimization of an urban microgrid operation including dispatched PV-based active generators*. IEEE Transactions on Sustainable Energy, 2014. **5**(4): p. 1397-1405.
 12. Li, Z., et al., *Transmission-constrained unit commitment considering combined electricity and district heating networks*. IEEE Transactions on Sustainable Energy, 2016. **7**(2): p. 480-492.
 13. Gu, Z., et al., *Operation optimization of integrated power and heat energy systems and the benefit on wind power accommodation considering heating network constraints*. Proc. CSEE, 2015. **35**(14): p. 3596-3604.
 14. Gu, W., et al., *Optimal operation for integrated energy system considering thermal inertia of district heating network and buildings*. Applied Energy, 2017. **199**: p. 234-246.
 15. Tasdighi, M., H. Ghasemi, and A. Rahimi-Kian, *Residential microgrid scheduling based on smart meters data and temperature dependent thermal load modeling*. IEEE Transactions on Smart Grid, 2014. **5**(1): p. 349-357.
 16. Wang, J., et al., *Optimal joint-dispatch of energy and reserve for CCHP-based microgrids*. IET Generation, Transmission & Distribution, 2017. **11**(3): p. 785-794.
 17. Anvari-Moghaddam, A., H. Monsef, and A. Rahimi-Kian, *Optimal smart home energy management considering energy saving and a comfortable lifestyle*. IEEE Transactions on Smart Grid, 2015. **6**(1): p. 324-332.
 18. Beraldi, P., D. Conforti, and A. Violi, *A two-stage stochastic programming model for electric energy producers*. Computers & Operations Research, 2008. **35**(10): p. 3360-3370.
 19. Wang, Q., Y. Guan, and J. Wang, *A chance-constrained two-stage stochastic program for unit commitment with uncertain wind power output*. IEEE Transactions on Power Systems, 2012. **27**(1): p. 206-215.
 20. Su, W., J. Wang, and J. Roh, *Stochastic Energy Scheduling in Microgrids With Intermittent Renewable Energy Resources*. IEEE Transactions on Smart Grid, 2014. **5**(4): p. 1876-1883.
 21. Zhou, X., T. Guo, and Y. Ma. *An overview on microgrid technology*. in *2015 IEEE international conference on mechatronics and automation (ICMA)*. 2015. IEEE.
-

22. V.-H. Bui, A.H., H.-M. Kim, *A multiagent-based hierarchical energy management strategy for multi-microgrids considering adjustable power and demand response*. IEEE Transactions on Smart Grid, 2016. **9**(2): p. 1323-1333.
23. Basu, A.K., et al., *Planned scheduling for economic power sharing in a CHP-based micro-grid*. IEEE Transactions on Power systems, 2012. **27**(1): p. 30.
24. Wesoff, E., *IEA: Global Installed PV Capacity Leaps to 303 Gigawatts*. 2017: greentechmedia.
25. Barbir, F. and T. Gomez, *Efficiency and economics of proton exchange membrane (PEM) fuel cells*. International Journal of Hydrogen Energy, 1997. **22**(10-11): p. 1027-1037.
26. Tsikalakis, A.G. and N.D. Hatziaargyriou. *Centralized control for optimizing microgrids operation*. in *2011 IEEE power and energy society general meeting*. 2011. IEEE.
27. Wei, G., et al., *Optimal configuration and analysis of combined cooling, heating, and power microgrid with thermal storage tank under uncertainty*. Journal of Renewable & Sustainable Energy, 2015. **7**(1): p. 2125-2141.
28. Wang, J., et al., *Coordinated planning of multi-district integrated energy system combining heating network model*. Autom. Electric Power Syst, 2016. **40**: p. 17-24.
29. Fumo, N. and L.M. Chamra, *Analysis of combined cooling, heating, and power systems based on source primary energy consumption*. Applied Energy, 2010. **87**(6): p. 2023-2030.
30. Li, Z., et al., *Combined heat and power dispatch considering pipeline energy storage of district heating network*. IEEE Transactions on Sustainable Energy, 2016. **7**(1): p. 12-22.
31. ZHAO Bo, W.C., ZHANG Xuesong, *A Survey of Suitable Energy Storage for Island-Stand alone Microgrid and Commercial Operation Mode*. Automation of Electric Power Systems. **37**(4): p. 21-27.
32. Liu, T. and D. Jiang, *Economic operation of microgrid based on operation mode optimization of energy storage unit*. Power System Technology, 2012. **36**(1): p. 45-50.

33. Balijepalli, V.M., et al. *Review of demand response under smart grid paradigm.* in *ISGT2011-India*. 2011. IEEE.
34. Brahman, F., M. Honarmand, and S. Jadid, *Optimal electrical and thermal energy management of a residential energy hub, integrating demand response and energy storage system.* *Energy and Buildings*, 2015. **90**: p. 65-75.
35. Zhang, C., et al., *Robust operation of microgrids via two-stage coordinated energy storage and direct load control.* *IEEE Transactions on Power Systems*, 2017. **32**(4): p. 2858-2868.
36. Baran, M.E. and F.F. Wu, *Network reconfiguration in distribution systems for loss reduction and load balancing.* *IEEE Transactions on Power delivery*, 1989. **4**(2): p. 1401-1407.
37. Palensky, P. and D. Dietrich, *Demand side management: Demand response, intelligent energy systems, and smart loads.* *IEEE transactions on industrial informatics*, 2011. **7**(3): p. 381-388.
38. Carrasco, J.M., et al., *Power-electronic systems for the grid integration of renewable energy sources: A survey.* *IEEE Transactions on Industrial Electronics*, 53 (4), 1002-1016., 2006.
39. Quelhas, A., et al., *A multiperiod generalized network flow model of the US integrated energy system: Part I—Model description.* *IEEE Transactions on Power Systems*, 2007. **22**(2): p. 829-836.
40. Quelhas, A. and J.D. McCalley, *A multiperiod generalized network flow model of the US integrated energy system: Part II—simulation results.* *IEEE Transactions on Power Systems*, 2007. **22**(2): p. 837-844.
41. Chen, C., et al., *Smart energy management system for optimal microgrid economic operation.* *IET renewable power generation*, 2011. **5**(3): p. 258-267.
42. Vasebi, A., M. Fesanghary, and S. Bathaee, *Combined heat and power economic dispatch by harmony search algorithm.* *International Journal of Electrical Power & Energy Systems*, 2007. **29**(10): p. 713-719.
43. Amini, M.H., et al., *Demand Response in Future Power Networks: Panorama and State-of-the-art*, in *Sustainable Interdependent Networks II*. 2019, Springer. p. 167-191.

44. Chen, Z., L. Wu, and Y. Fu, *Real-time price-based demand response management for residential appliances via stochastic optimization and robust optimization*. IEEE Transactions on Smart Grid, 2012. **3**(4): p. 1822-1831.
45. Zhang, C., et al., *Robust coordination of distributed generation and price-based demand response in microgrids*. IEEE Transactions on Smart Grid, 2017.
46. Bahrami, S., et al., *A decentralized energy management framework for energy hubs in dynamic pricing markets*. IEEE Transactions on Smart Grid, 2018. **9**(6): p. 6780-6792.
47. Xu, F.Y. and L.L. Lai, *Novel active time-based demand response for industrial consumers in smart grid*. IEEE Transactions on Industrial Informatics, 2015. **11**(6): p. 1564-1573.
48. Ma, K., G. Hu, and C.J. Spanos, *A cooperative demand response scheme using punishment mechanism and application to industrial refrigerated warehouses*. IEEE Transactions on Industrial Informatics, 2015. **11**(6): p. 1520-1531.
49. Kilkki, O., A. Alahäivälä, and I. Seilonen, *Optimized control of price-based demand response with electric storage space heating*. IEEE Transactions on industrial Informatics, 2015. **11**(1): p. 281-288.
50. Ding, Y.M., S.H. Hong, and X.H. Li, *A demand response energy management scheme for industrial facilities in smart grid*. IEEE Transactions on Industrial Informatics, 2014. **10**(4): p. 2257-2269.
51. Mathieu, J.L., et al., *Quantifying changes in building electricity use, with application to demand response*. IEEE Transactions on Smart Grid, 2011. **2**(3): p. 507-518.
52. Deng, R., et al., *A survey on demand response in smart grids: Mathematical models and approaches*. IEEE Transactions on Industrial Informatics, 2015. **11**(3): p. 570-582.
53. Mohajeryami, S., et al., *A novel economic model for price-based demand response*. Electric Power Systems Research, 2016. **135**: p. 1-9.
54. Thimmapuram, P.R., et al. *Modeling and simulation of price elasticity of demand using an agent-based model*. in *2010 Innovative Smart Grid Technologies (ISGT)*. 2010. IEEE.

55. P. He, e.a., *District heating engineering*. Architecture & Building Press: Beijing, China, 2009.
56. Zhang, C., Y. Xu, and Z.Y. Dong, *Probability-Weighted Robust Optimization for Distributed Generation Planning in Microgrids*. IEEE Transactions on Power Systems, 2018. **33**(6): p. 7042-7051.
57. Tascikaraoglu, A., et al., *An adaptive load dispatching and forecasting strategy for a virtual power plant including renewable energy conversion units*. Applied Energy, 2014. **119**: p. 445-453.
58. Zhang, R., et al., *Short-term load forecasting of Australian National Electricity Market by an ensemble model of extreme learning machine*. IET Generation, Transmission & Distribution, 2013. **7**(4): p. 391-397.
59. Niknam, T., M. Zare, and J. Aghaei, *Scenario-based multiobjective volt/var control in distribution networks including renewable energy sources*. IEEE Transactions on Power Delivery, 2012. **27**(4): p. 2004-2019.
60. Alipour, M., B. Mohammadi-Ivatloo, and K. Zare, *Stochastic scheduling of renewable and CHP-based microgrids*. IEEE Transactions on Industrial Informatics, 2015. **11**(5): p. 1049-1058.
61. Wu, L., M. Shahidehpour, and T. Li, *Stochastic security-constrained unit commitment*. IEEE Transactions on Power Systems, 2007. **22**(2): p. 800-811.
62. Xu, Y., et al., *Multi-timescale coordinated voltage/var control of high renewable-penetrated distribution systems*. IEEE Transactions on Power Systems, 2017. **32**(6): p. 4398-4408.